

Relativistic calculations of the charge-transfer probabilities and cross sections for low-energy collisions of H-like ions with bare nuclei

I. I. Tupitsyn,¹ Y. S. Kozhedub,¹ V. M. Shabaev,¹ G. B. Deyneka,²
S. Hagmann,³ C. Kozhuharov,³ G. Plunien,⁴ and Th. Stöhlker^{3,5,6}

¹ *Department of Physics, St. Petersburg State University,
Ulianovskaya 1, Petrodvorets, 198504 St. Petersburg, Russia*

² *St. Petersburg State University of Information Technologies,
Mechanics and Optics, Kronverk av. 49, 197101 St. Petersburg, Russia*

³ *GSI Helmholtzzentrum für Schwerionenforschung GmbH,
Planckstrasse 1, D-64291 Darmstadt, Germany*

⁴ *Institut für Theoretische Physik, Technische Universität Dresden,
Mommsenstraße 13, D-01062 Dresden, Germany*

⁵ *Physikalisches Institut, Universität Heidelberg,
Philosophenweg 12, D-69120 Heidelberg, Germany*

⁶ *Helmholtz-Institut Jena, D-07743 Jena, Germany*

Abstract

A new method for solving the time-dependent two-center Dirac equation is developed. The time-dependent Dirac wave function is represented as a sum of atomic-like Dirac-Sturm orbitals, localized at the ions. The atomic orbitals are obtained by solving numerically the finite-difference one-center Dirac and Dirac-Sturm equations with the potential which is the sum of the exact reference-nucleus potential and a monopole-approximation potential from the other nucleus. An original procedure to calculate the two-center integrals with these orbitals is proposed. The approach is tested by calculations of the charge transfer and ionization cross sections for the $H(1s)$ –proton collisions at proton energies from 1 keV to 100 keV. The obtained results are compared with related experimental and other theoretical data. To investigate the role of the relativistic effects, the charge transfer cross sections for the $Ne^{9+}(1s)$ – Ne^{10+} (at energies from 0.1 to 10 MeV/u) and $U^{91+}(1s)$ – U^{92+} (at energies from 6 to 10 MeV/u) collisions are calculated in both relativistic and nonrelativistic cases.

PACS numbers: 34.10.+x, 34.50.-s, 34.70.+e

I. INTRODUCTION

Since the pioneering works [1–3], where the oscillatory behavior of the resonance charge-transfer probability for low-energy collisions was predicted, numerous publications have been devoted to the theoretical investigations of the charge-transfer, excitations and ionization in the $\text{H}(1s)\text{-H}^+$ collisions (see, e.g., reviews [4–6]). Nonrelativistic two-center finite basis set calculations have been carried out in Refs. [7–13]. Nonrelativistic three-dimensional lattice methods in the position and momentum spaces have been applied for the time-dependent Schrödinger equation in Refs. [14–18]. Within the nonrelativistic approach, the probabilities and cross-sections for a homonuclear collision $\text{A}^{(Z-1)+}(1s)\text{-A}^{Z+}$ for the nuclear charge $Z > 1$ can be easily obtained by scaling to the $\text{H}(1s)\text{-H}^+$ collision. In the straight-line trajectory approximation, the cross section $\sigma(Z, v)$ scales exactly as $\sigma(Z, v) = \sigma(1, v/Z)/Z^2$ [4, 19], where v is the projectile velocity. This scaling law is not valid, however, in the relativistic theory.

Collisions involving highly charged ions provide tests of relativistic and quantum electrodynamics effects in the scattering theory [20–22]. The study of such processes can provide also a unique tool to probe the quantum electrodynamics (QED) in the supercritical Coulomb field, if the total charge of the colliding ions $Z = Z_A + Z_B$ is larger than the critical one $Z_c = 173$ (see, e.g., Refs. [23–26] and references therein). In the presence of such a field the energy of the one-electron $1\sigma_+$ state of the quasi-molecule can reach the negative-energy Dirac continuum, when the distance R between target ion A and projectile ion B becomes equal to the critical value R_c . For the distance R less than R_c the ground state level dives into the negative-continuum spectrum. In the $\text{U}^{91+}(1s)\text{-U}^{92+}$ collision the critical radius for the point nucleus case was found to be $R_c = 36.8$ fm [27].

To date various approaches were developed to treat the heavy-ion collisions [28]. In Refs. [29–36], the two- and three-dimensional numerical lattice methods were employed to solve the time-dependent Dirac equation at high energies. In Refs. [37–40], high energy relativistic collisions of heavy ions were considered using the basis set approach, in which the time-dependent wave function was expanded in terms of the atomic eigenstates of the projectile and the target. For internuclear distances smaller than about 1000 fm some effects can also be evaluated within so-called monopole approximation, which accounts only for the spherically-symmetric part of the two-center potential [41–43]. The atomic processes such as excitation, ionization and charge transfer in relativistic atomic collisions involving heavy

and highly-charged projectile ions with energies ranging from 100 MeV/u upward were studied in Refs. [20, 34, 36, 44–46] and references therein.

In the present work, we develop a new method for solving the two-center stationary and time-dependent Dirac equations. The wave functions are expanded in terms of the Dirac and Dirac-Sturm basis functions, which are central-field 4-component Dirac bispinors centered at the ions. The radial parts of these orbitals are obtained by solving numerically the finite-difference radial one-center Dirac and Dirac-Sturm equations. In the nonrelativistic calculations of atoms and molecules, so-called Coulomb-Sturmian basis set was introduced in Ref. [47]. The Hartree-Fock calculations of atoms with this basis were considered by many authors (see, e.g., Ref. [48]). The relativistic Coulomb-Sturmian basis was employed in the papers [49–52]. In the present paper we use a non-Coulomb relativistic Sturm basis set, which is obtained by solving numerically the Dirac-Sturm equations with a special choice of the weight function, that was proposed in Refs. [53, 54]. This allows us to include any central-field potential in the radial equations for the large and small components of the basis functions. In particular, the Coulomb potential of the other ion can be included in the radial equations within the monopole approximation. The basis set constructed in this way is described in detail in section II B.

Calculations of two-center integrals with the basis functions obtained require using special tools. In the nonrelativistic case, a special symmetrical procedure for such calculations, based on the Löwdin reexpansion [55], was developed in Refs. [56, 57]. In section II C, we generalize this procedure to the relativistic case.

To test the quality of the two-center expansion described above we perform relativistic calculations of the ground-state energy of molecular ion H_2^+ and one-electron quasi-molecule Th_2^{179+} at the “chemical” distance $R = 2/Z$ a.u. and compare the results with high-precision calculations of Refs. [58, 59]. We also calculate the ground-state energy as a function of the internuclear distance R and the critical radii R_c for a number of one-electron quasi-molecules, including U_2^{183+} . Most calculations of the critical distances R_c presented in the literature were performed either for the point-nucleus model [27, 60, 61] or with a crude estimate of the nuclear-size effect [62–64]. We calculate the critical distances for both point and extended nucleus models using the same basis set expansion. The obtained results and comparison with the calculations by other authors are presented in section III B.

The classical Rutherford trajectories [25] of the projectile and target ions are obtained by numerical solution of the Newton’s equations. The Born-Oppenheimer approximation is used to separate the mo-

tion of the electron and the nuclei. The magnetic interaction between the electron and the moving ions is neglected, because of low velocity of the projectile with respect to the target. The time-dependent Dirac equation for the electron is solved using the two-center basis set expansion. The expansion coefficients can be defined employing, e.g., the Crank-Nicholsen propagation scheme [65] or the split-operator method [66]. These methods conserve the norm of the time-dependent wave function at each time step, since the Crank-Nicholsen operator and the split-operator are unitary. However, in this work we use the direct evolution exponential operator method, which is more stable compared to the others. To obtain the matrix of the exponential operator in the finite basis set one has to diagonalize the generalized Hamiltonian matrix at each step of time. Since our basis set is not too large, the diagonalization procedure is not too time consuming. The amplitudes of the charge transfer to different bound states of the projectile ion are calculated nonperturbatively by projecting the time-dependent wave function onto the moving Dirac orbitals of the projectile.

In section III C we present the results of the relativistic calculations of the charge-transfer probabilities and cross sections for the $\text{H}(1s)\text{--H}^+$, $\text{Ne}^{9+}(1s)\text{--Ne}^{10+}$, $\text{Xe}^{53+}(1s)\text{--Xe}^{54+}$, and $\text{U}^{91+}(1s)\text{--U}^{92+}$ low-energy collisions. All the calculations are performed in the laboratory frame S , that is defined to be at rest with respect to the initial target position. The $\text{H}(1s)\text{--H}^+$ collision is considered in section III C 1. Since the relativistic effects in this collision are negligible, the results of our calculations can be compared with nonrelativistic data obtained by other authors (section III C 1). The role of the relativistic effects is investigated in sections III C 2, III C 3, and III C 4, where the relativistic and nonrelativistic calculations of the charge-transfer probabilities and cross sections are performed for higher- Z ions.

II. THEORY

A. Two-center Dirac equation in the finite basis set

1. Two-center expansion

Within the Born-Oppenheimer approximation, the motion of the electron is considered as a motion in the field of the two nuclei being at given positions (the stationary case) or moving along the classical trajectories (the non-stationary case). Let \mathbf{R}_A and \mathbf{R}_B are the positions of the target (A) and projectile (B) nuclei, respectively. The time-dependent $\Psi(\mathbf{r}, t)$ and stationary $\psi(\mathbf{r})$ wave functions are

the solutions of the time-dependent and stationary Dirac equations, respectively. In the atomic units ($\hbar = m = e = 1$), these equations are given by

$$i \frac{\partial \Psi(\mathbf{r}, t)}{\partial t} = \hat{h}_D \Psi(\mathbf{r}, t), \quad \hat{h}_D \psi_n(\mathbf{r}) = \varepsilon_n \psi_n(\mathbf{r}). \quad (1)$$

Here ε_n is the energy of the stationary state and the \hat{h}_D is the two-center Dirac Hamiltonian defined by

$$\hat{h}_D = c(\boldsymbol{\alpha} \cdot \mathbf{p}) + \beta c^2 + V_{AB}(\mathbf{r}), \quad (2)$$

where c is the speed of light, $\boldsymbol{\alpha}, \beta$ are the Dirac matrices, and

$$V_{AB}(\mathbf{r}) = V_{\text{nucl}}^A(\mathbf{r}_A) + V_{\text{nucl}}^B(\mathbf{r}_B), \quad \mathbf{r}_A = \mathbf{r} - \mathbf{R}_A, \quad \mathbf{r}_B = \mathbf{r} - \mathbf{R}_B, \quad (3)$$

$$V_{\text{nucl}}(\mathbf{r}) = \begin{cases} -Z/r & \text{for the point nucleus} \\ \int d^3\mathbf{r}' \frac{\rho_{\text{nucl}}(\mathbf{r}')}{|\mathbf{r} - \mathbf{r}'|} & \text{for the extended nucleus.} \end{cases} \quad (4)$$

The nuclear charge density $\rho_{\text{nucl}}(\mathbf{r})$ is defined by the nuclear model. In this paper we will use the Fermi model for the nuclear charge distribution.

Here and in what follows we consider only the electric part of the classical electromagnetic interaction between the electron and the moving nuclei neglecting the magnetic interaction ($e/c \mathbf{A}(\mathbf{r})$), which is small for low-energy collisions.

The two-center expansion of the stationary wave function $\psi_n(\mathbf{r})$ and the time-dependent wave function $\Psi(\mathbf{r}, t)$ can be written in the form

$$\begin{cases} \psi_n(\mathbf{r}) = \sum_{\alpha=A,B} \sum_a c_{\alpha a}^n \varphi_{\alpha, a}(\mathbf{r} - \mathbf{R}_\alpha) \\ \Psi(\mathbf{r}, t) = \sum_{\alpha=A,B} \sum_a C_{\alpha a}(t) \varphi_{\alpha, a}(\mathbf{r} - \mathbf{R}_\alpha(t)), \end{cases} \quad (5)$$

where index $\alpha = A, B$ enumerates the centers, index a enumerates basis functions at the given center, and $\varphi_{\alpha, a}(\mathbf{r} - \mathbf{R}_\alpha)$ is the central-field bispinor, centered at point α . The coefficients $c_{\alpha a}^n$ of the expansion (5) for the stationary wave function $\psi_n(\mathbf{r})$ can be obtained from the generalized eigenvalue equation

$$\sum_k H_{jk} c_k^n = \varepsilon_n \sum_k S_{jk} c_k^n, \quad (6)$$

where indexes j and k enumerate the basis functions of both centers, and the matrix elements of H and S are given by

$$H_{jk} = \langle j | \hat{h}_D | k \rangle, \quad S_{jk} = \langle j | k \rangle. \quad (7)$$

The expansion coefficients $C_{a\alpha}(t)$ of the time-dependent wave function $\Psi(\mathbf{r}, t)$ can be obtained by solving the linear system of first-order differential equations

$$i \sum_k S_{jk} \frac{dC_k(t)}{dt} = \sum_k (H_{jk} - T_{jk}) C_k(t) . \quad (8)$$

The matrix elements of T are given by

$$T_{jk} = i \langle j | \frac{\partial}{\partial t} | k \rangle = T_{kj}^* + i \frac{\partial}{\partial t} S_{jk} . \quad (9)$$

Obviously the matrix T is non-Hermitian, if the overlapping matrix S depends on time.

The functions φ_α depend on time due to two reasons. First, the basis functions centered at the target and projectile nuclei move together with the nuclei. Second, the basis functions depend parametrically on the distance between the nuclei, since their radial parts are obtained from the radial equations, where for each center the potential of the other nucleus is included in the so-called monopole approximation (see section II B). Therefore, the time derivative of the basis function can be divided into two parts

$$\langle j | \frac{\partial}{\partial t} | k \rangle = \frac{dR}{dt} \langle \varphi_j | \frac{\partial \varphi_k}{\partial R} \rangle - \mathbf{v}_{\alpha_k} \cdot \langle \varphi_j | \nabla | \varphi_k \rangle , \quad (10)$$

where $\mathbf{v}_\alpha = d\mathbf{R}_\alpha/dt$ is the velocity of the ion α .

2. Trajectories of nuclear motion

In the ion-ion collisions the internuclear distance vector $\mathbf{R} = \mathbf{R}_B - \mathbf{R}_A$, the length R of vector \mathbf{R} , the target velocity (\mathbf{v}_A), and the projectile velocity (\mathbf{v}_B) are time dependent. This dependence is defined by the trajectories of the nuclear motion. In low-energy collisions the nuclear trajectories can be obtained by solving classical non-relativistic Newton's equations of motion. In the case of point charges this solution is well-known Rutherford hyperbola (see Fig. 1), which can be given in the parametric representation by the equations [25]

$$\begin{cases} R = a (\varepsilon \cosh \xi + 1) \\ t = \frac{a}{v_0} (\varepsilon \sinh \xi + \xi) , \end{cases} \quad (11)$$

where $\xi \in (-\infty, \infty)$,

$$a = \frac{Z_A Z_B e^2}{M_r v_0^2} , \quad \varepsilon = \left(1 + \frac{b^2}{a^2} \right)^{1/2} , \quad (12)$$

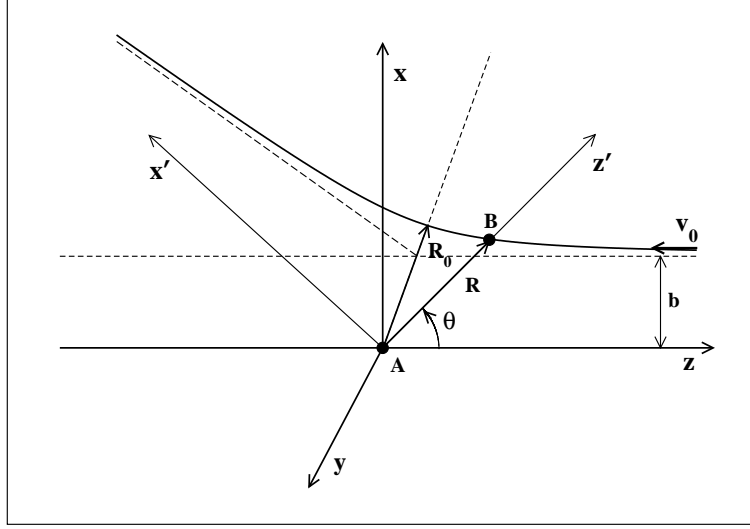


FIG. 1: The hyperbolic Rutherford trajectory (b is the impact parameter, R_0 is the minimal distance between target A and projectile B, v_0 is the initial projectile velocity). The coordinate system $S_t = (x, y, z)$ is defined with respect to the moving target ion.

v_0 is the initial velocity of the projectile, b is the impact parameter, and M_r is the reduced ion mass. In the coordinate system $S_t = (x, y, z)$, which is shown in Fig. 1, the X and Z components of the internuclear distance vector \mathbf{R} are given by

$$\begin{cases} Z = R \cos \theta \\ X = R \sin \theta \end{cases}, \quad \text{where } \theta = 2 \arctg \left[\frac{\sqrt{\varepsilon^2 - 1} (\text{th}(\xi/2) + 1)}{(\varepsilon + 1) - (\varepsilon - 1) \text{th}(\xi/2)} \right]. \quad (13)$$

The angle θ is related to the scattering angle Θ_∞ by $\Theta_\infty = \pi - \theta(t = \infty)$.

3. Time-dependent matrix Dirac equation

In this work the two-center basis set φ_j is not orthonormal. Let us consider the transformation of the basis set φ_j to the orthonormal basis φ_j^L by a matrix L^{-1}

$$\varphi_j^L = \sum_k L_{kj}^{-1} \varphi_k, \quad \varphi_j = \sum_k L_{kj} \varphi_k^L. \quad (14)$$

Then the positive-defined matrix S can be represented as the product of L^+ and L :

$$S = L^+ L, \quad S_{jk}^L = \langle \varphi_j^L | \varphi_k^L \rangle = (L^{-1+} S L^{-1})_{jk} = \delta_{j,k}. \quad (15)$$

If the matrix L is an upper-triangle matrix, then the decomposition (15) is so-called Cholesky factorization [67]. The expansion of the time-dependent wave function over the orthonormal basis φ_j^L is given by

$$\Psi(\mathbf{r}, t) = \sum_{\alpha=A,B} \sum_a C_{\alpha,a}^L(t) \varphi_{\alpha,a}^L(\mathbf{r} - \mathbf{R}_\alpha(t), t), \quad (16)$$

where $\mathbf{C}^L = L \mathbf{C}$.

The time-dependent Dirac equation in the basis φ_j^L can be written in the form

$$i \frac{d\mathbf{C}^L(t)}{dt} = M \mathbf{C}^L(t), \quad (17)$$

where $M = H^L - T^L$, the Hermitian Hamiltonian matrix H^L is

$$H_{ij}^L = \langle \varphi_i | \hat{H} | \varphi_j \rangle = (L^{-1+} H L^{-1})_{ij}, \quad (18)$$

and the matrix T^L is defined by

$$T_{ij}^L = \langle \varphi_i^L | \hat{T} | \varphi_j^L \rangle = (L^{-1+} T L^{-1})_{ij} + i \left(L \frac{dL^{-1}}{dt} \right)_{ij} = \left(L^{-1+} \left[T - i L^+ \frac{dL}{dt} \right] L^{-1} \right)_{ij}. \quad (19)$$

It should be noted that matrix T^L is Hermitian, in contrast to the matrix T defined by Eq. (9). Therefore, the matrix M is also Hermitian.

The time-dependent matrix equation (17) can be considered as a linear system of the first-order differential equations at the range of time $t \in (-\infty, \infty)$. We assume that at the initial moment of time ($t \rightarrow -\infty$) the electron is localized on the target in the $1s$ state and the projectile is the bare nucleus. Then, the wave function $\Psi(\mathbf{r}, t)$ at $t \rightarrow -\infty$ is given by

$$\Psi(\mathbf{r}, t) \Big|_{t \rightarrow -\infty} = \psi_{1s}(\mathbf{r}). \quad (20)$$

If the Dirac $1s$ -target wave function $\psi_{1s}(\mathbf{r})$ is included in the basis set, the initial conditions for the expansion coefficients can be written as

$$C_j^L(t) \Big|_{t \rightarrow -\infty} = C_j(t) \Big|_{t \rightarrow -\infty} = \delta_{j,1s}. \quad (21)$$

Equation (17) is solved numerically, using approximate evolution operator

$$\mathbf{C}^L(t + \Delta t) = e^{-i\overline{M}\Delta t} \mathbf{C}^L(t) + O(\Delta^3 t), \quad (22)$$

where Hermitian matrix \overline{M} is chosen as

$$\overline{M} = M(t + \Delta t/2). \quad (23)$$

Since the approximate evolution operator $U(t) = \exp(-i\overline{M}t)$ is unitary, the time-dependent wave function conserves the norm at each time step

$$\langle \Psi(\mathbf{r}, t) | \Psi(\mathbf{r}, t) \rangle = \sum_j |C_j^L(t)|^2 = 1. \quad (24)$$

The matrix $e^{-i\overline{M}t}$ is calculated at each time step using the eigen decomposition of matrix \overline{M}

$$\overline{M} = V \Lambda V^+, \quad (25)$$

where Λ is a diagonal matrix and columns of matrix V are the eigenvectors of \overline{M} . Then one obtains

$$e^{-i\overline{M}t} = V e^{-i\Lambda t} V^+. \quad (26)$$

The time grid points t_i are chosen as $t_i = a/v_0 (\varepsilon \sinh \xi_i + \xi_i)$, where the parameter ξ runs a uniform grid. The grid points R_i can be obtained using equation (11).

B. Basis functions

In our approach the basis set contains Dirac and Dirac-Sturm orbitals. The Dirac-Sturm orbitals can be considered as pseudo-states, which should be included in the basis to take into account the contribution of the positive- and negative-energy Dirac continuum. Both types of basis functions $\varphi_{\alpha a}$ are the central field Dirac bispinors centered at the position \mathbf{R}_α ($\alpha = A, B$)

$$\varphi_{n\kappa m}(\mathbf{r}) = \begin{pmatrix} \frac{P_{n\kappa}(r)}{r} \chi_{\kappa m}(\Omega, \sigma) \\ i \frac{Q_{n\kappa}(r)}{r} \chi_{-\kappa m}(\Omega, \sigma) \end{pmatrix}, \quad (27)$$

where $P_{n\kappa}(r)$ and $Q_{n\kappa}(r)$ are large and small radial components, respectively, and $\kappa = (-1)^{l+j+1/2}(j+1/2)$ is the relativistic angular quantum number. The large and small radial orbital components are obtained by solving numerically the Dirac or Dirac-Sturm equations in the central field potential $V(r)$.

The Dirac equation is given by

$$\begin{cases} c \left(-\frac{d}{dr} + \frac{\kappa}{r} \right) Q_{n\kappa}(r) + (V(r) + c^2) P_{n\kappa}(r) = \varepsilon_{n\kappa} P_{n\kappa}(r) \\ c \left(\frac{d}{dr} + \frac{\kappa}{r} \right) P_{n\kappa}(r) + (V(r) - c^2) Q_{n\kappa}(r) = \varepsilon_{n\kappa} Q_{n\kappa}(r). \end{cases} \quad (28)$$

The radial components of the Dirac-Sturm orbitals which we denote by $\overline{P}_{n\kappa}(r)$ and $\overline{Q}_{n\kappa}(r)$ are the solutions of the Dirac-Sturm generalized eigenvalue equation

$$\begin{cases} c \left(-\frac{d}{dr} + \frac{\kappa}{r} \right) \overline{Q}_{n\kappa}(r) + (V(r) + c^2 - \varepsilon_{n_0\kappa}) \overline{P}_{n\kappa}(r) = \lambda_{n\kappa} W_{\kappa}(r) \overline{P}_{n\kappa}(r) \\ c \left(\frac{d}{dr} + \frac{\kappa}{r} \right) \overline{P}_{n\kappa}(r) + (V(r) - c^2 - \varepsilon_{n_0\kappa}) \overline{Q}_{n\kappa}(r) = \lambda_{n\kappa} W_{\kappa}(r) \overline{Q}_{n\kappa}(r). \end{cases} \quad (29)$$

Here $\lambda_{n\kappa}$ can be considered as the eigenvalue of the Dirac-Sturm operator and $W_{\kappa}(r)$ is a constant sign weight function. The energy $\varepsilon_{n_0\kappa}$ is fixed in the Dirac-Sturm equation. If $W(r) \rightarrow 0$ at $r \rightarrow \infty$, all Sturmian functions have the same asymptotic at $r \rightarrow \infty$. It is clear that for $\lambda_{n\kappa} = 0$ the Sturmian function coincides with the reference Dirac orbital which has the radial parts $P_{n_0\kappa}(r)$ and $Q_{n_0\kappa}(r)$. The widely known choice of the weight function is $W(r) = 1/r$, which leads to the well known 'charge quantization' $Z_{n\kappa}^* = Z + \lambda_{n\kappa}$. The main advantage of this choice for the Coulomb potential $V(r) = -Z/r$ is that the Coulomb-Sturmian orbitals can be given in an analytical form. This is not the case, however, for the non-Coulomb potential $V(r)$. In the relativistic case the choice $W(r) = 1/r$ is not very successful, because of the incorrect behavior of the Coulomb-Sturmian orbitals at $r \rightarrow 0$. For this reason the standard form of the equation has to be modified [50, 68, 69].

In our calculations we use the following weight function

$$W_{\kappa}(r) = -\frac{1 - \exp(-(\alpha_{\kappa} r)^2)}{(\alpha_{\kappa} r)^2}. \quad (30)$$

In contrast to $1/r$, this weight function is regular at origin. It is well-known that the Sturmian operator is Hermitian and does not contain continuum spectra, in contrast to the Dirac operator. Therefore, the set of the Sturmian eigenfunctions forms the discrete and complete basis set of one-electron wave functions.

The central-field potential $V(r)$ in equations (28) and (29) is arbitrary, and, therefore, it can be chosen to provide most appropriate Dirac and Dirac-Sturm basis orbitals. At short internuclear distances the wave function of the electron experiences the strong Coulomb field of both nuclei. To take into

account this effect we have included the Coulomb potential of the second ion in the total one center potential $V(r)$ in so-called monopole approximation. For instance, the total central-field potential $V^A(r)$ of the center A is given by

$$V^A(r) = V_{\text{nucl}}^A(r) + V_{\text{mon}}^B(r), \quad (31)$$

where $V_{\text{nucl}}^A(r)$ is the Coulomb potential of the nucleus A and $V_{\text{mon}}^B(r)$ is the spherically-symmetric part of the reexpansion of the potential $V_{\text{nucl}}^B(\mathbf{r} - \mathbf{R}_B)$ on the center A

$$V_{\text{mon}}^B(r) = \frac{1}{4\pi} \int d\Omega_A V_{\text{nucl}}^B(\mathbf{r} - \mathbf{R}_B). \quad (32)$$

For the point nucleus the potential $V_{\text{mon}}^B(r)$ is given by

$$V_{\text{mon}}^B(r) = \begin{cases} -\frac{Z_B}{r} & r \geq R \\ -\frac{Z_B}{R} & r < R. \end{cases} \quad (33)$$

C. Two-center integrals

The matrix elements of H and S (Eq. 7) are easily reduced to radial integrals [70], which are calculated by numerical integration in the radial semi-logarithmic grid [71].

Modified Löwdin reexpansion procedure

Two-center matrix elements are calculated using a symmetrical reexpansion procedure, proposed in Refs. [56, 57]. The reexpansion procedure is based on the technique developed by Löwdin [55]. We assume that in the local coordinate frame the z -axis is directed along the internuclear axis A – B (see Fig. 2). The following geometrical relations take place

$$\begin{aligned} \mathbf{r}_A &= \mathbf{r} - \mathbf{R}_A, & \mathbf{r}_B &= \mathbf{r} - \mathbf{R}_B, & \mathbf{R} &= \mathbf{R}_B - \mathbf{R}_A, \\ \cos \theta_A &= \frac{r_A^2 + R^2 - r_B^2}{2Rr_A}, & \cos \theta_B &= \frac{r_A^2 - R^2 - r_B^2}{2Rr_B}. \end{aligned} \quad (34)$$

Let the indexes a and b enumerate basis functions centered at the points A and B , respectively. The standard Löwdin reexpansion of the nonrelativistic central-field function $F_b(\mathbf{r}_B)$ centered at the point B

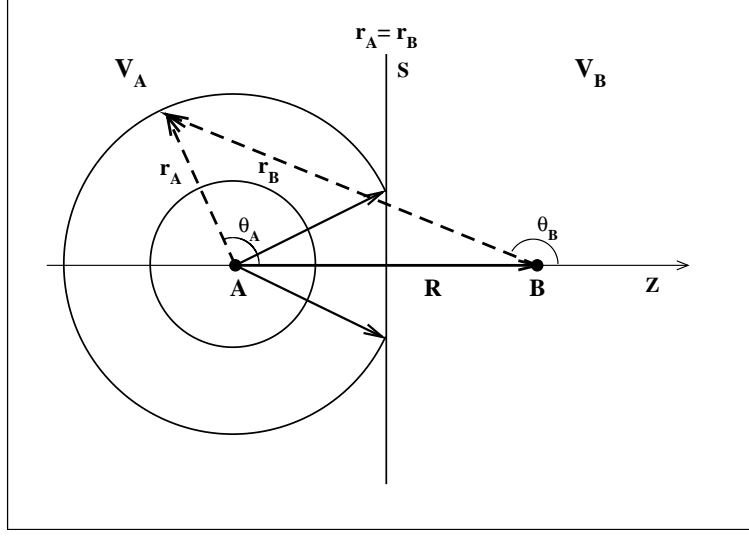


FIG. 2: Integration regions V_A and V_B .

in terms of the spherical harmonics $Y_{lm}(\mathbf{r}_A)$ centered at the point A can be written in the form [55, 72]

$$F_b(\mathbf{r}_B) = \frac{f_b(r_B)}{r_B} Y_{l_b m_b}(\theta_B, \varphi) = \frac{1}{r_A} \sum_{l=0}^{\infty} \alpha_{lm_b}(f_b, l_b | r_A) Y_{lm_b}(\theta_A, \varphi), \quad (35)$$

where $\alpha_{lm_b}(f_b, l_b | r_A)$ is so-called Löwdin α -function defined by

$$\alpha_{lm_b}(f_b, l_b | r_A) = \frac{K_{l_b m_b} K_{lm_b}}{R} \int_{|r_A - R|}^{|r_A + R|} f_b(r) P_{l_b}^{|m_b|} \left(\frac{r_A^2 - R^2 - r^2}{2rR} \right) P_l^{|m_b|} \left(\frac{r_A^2 + R^2 - r^2}{2r_A R} \right) dr. \quad (36)$$

Here $P_l^{|m|}$ is the standard associated Legendre polynomial and K_{lm} is the normalization constant

$$K_{lm} = \sqrt{\frac{2l+1}{2} \frac{(l-|m|)!}{(l+|m|)!}}. \quad (37)$$

Similarly, the function $F_a(\mathbf{r}_A)$ centered at point A can be expanded in spherical harmonics $Y_{lm}(\theta_B, \varphi)$ centered at the point B .

When the logarithmic or semi-logarithmic grid is used the radial grid step increases with increasing radius r_A . Therefore, the Löwdin reexpansion procedure becomes unstable and poorly convergent for the values of radius r_A in the region near $r_A = R$, especially for the oscillating and strongly localized atomic-like wave functions. In addition, the Löwdin procedure is not symmetric with respect to the centers A and B .

To improve the convergence we modified the standard Löwdin reexpansion procedure by dividing the range of the integration into two regions V_A and V_B as shown in Fig. 2. The region V_A contains ion

A and the region V_B contains ion B . The dividing of the integration area into two parts can be done, for example, by a plane passing through the center of the segment (AB) . We apply the reexpansion procedure only to the "tails" of the wave functions occurring in a given region. To describe this procedure we introduce the step-wise functions $\Theta_A(\mathbf{r})$ and $\Theta_B(\mathbf{r})$ by

$$\Theta_A(\mathbf{r}) = \begin{cases} 1 & \mathbf{r} \in V_A \\ 0 & \mathbf{r} \in V_B, \end{cases} \quad \Theta_B(\mathbf{r}) = \begin{cases} 0 & \mathbf{r} \in V_A \\ 1 & \mathbf{r} \in V_B, \end{cases} \quad (38)$$

and rewrite the product of the functions centered at the different points in the following way

$$F_a(\mathbf{r}_A) \cdot F_b(\mathbf{r}_B) = F_a(\mathbf{r}_A) \cdot (F_b(\mathbf{r}_B) \Theta_A(\mathbf{r})) + (F_a(\mathbf{r}_A) \Theta_B(\mathbf{r})) \cdot F_b(\mathbf{r}_B). \quad (39)$$

The reexpansion of the function tail $F_b(\mathbf{r}_B) \Theta_A(\mathbf{r})$ centered at B onto center A has the form

$$F_b(\mathbf{r}_B) \Theta_A(\mathbf{r}) = \frac{f_b(r_B)}{r_B} Y_{l_b m_b}(\theta_B, \varphi) \Theta_A(\mathbf{r}) = \frac{1}{r_A} \sum_l \bar{\alpha}_{l m_b}(f_b, l_b | r_A) \cdot Y_{l m_b}(\theta_A, \varphi), \quad (40)$$

where

$$\bar{\alpha}_{l m_b}(f_b, l_b | r_A) = \frac{K_{l_b m_b} K_{l m_b}}{R} \int_{r_A^>}^{|r_A+R|} f_b(r) P_{l_b}^{|m_b|} \left(\frac{r_A^2 - R^2 - r^2}{2rR} \right) P_l^{|m_b|} \left(\frac{r_A^2 + R^2 - r^2}{2r_A R} \right) dr \quad (41)$$

and $r_A^> = \max\{r_A, |r_A - R|\}$.

In the relativistic case the spin-angular part $\chi_{\kappa m}$ of the large and small components of the central-field wave function is the Pauli spinor [73]

$$\chi_{\kappa \mu}(\mathbf{r}, \sigma) = \chi_{l j \mu}(\mathbf{r}, \sigma) = \sum_{m, m_s} C_{l m, \frac{1}{2}, m_s}^{j \mu} Y_{l m}(\mathbf{r}) \Phi_{m_s}(\sigma), \quad (42)$$

where $C_{l m, \frac{1}{2}, m_s}^{j \mu}$ are the Clebsch-Gordan coefficients [74] and $\Phi_{m_s}(\sigma)$ is a spin function.

The symmetric reexpansion of the relativistic wave function "tails" onto centers A and B can be written in the form

$$\begin{pmatrix} \frac{P_b(r_B)}{r_B} \chi_{\kappa_b \mu_b}(\mathbf{r}_B) \\ i \frac{Q_b(r_B)}{r_B} \chi_{-\kappa_b \mu_b}(\mathbf{r}_B) \end{pmatrix} \Theta_A(\mathbf{r}) = \sum_{\kappa} \begin{pmatrix} \frac{\bar{P}_{\kappa \mu_b}(b | r_A)}{r_A} \chi_{\kappa \mu_b}(\mathbf{r}_A) \\ i \frac{\bar{Q}_{-\kappa \mu_b}(b | r_A)}{r_A} \chi_{-\kappa \mu_b}(\mathbf{r}_A) \end{pmatrix} \quad (43)$$

and

$$\begin{pmatrix} \frac{P_a(r_A)}{r_A} \chi_{\kappa_a \mu_a}(\mathbf{r}_A) \\ i \frac{Q_a(r_A)}{r_A} \chi_{-\kappa_a \mu_a}(\mathbf{r}_A) \end{pmatrix} \Theta_B(\mathbf{r}) = \sum_{\kappa} (-1)^{l_a - l} \begin{pmatrix} \frac{\bar{P}_{\kappa \mu_a}(a | r_B)}{r_B} \chi_{\kappa \mu_a}(\mathbf{r}_B) \\ i \frac{\bar{Q}_{-\kappa \mu_a}(a | r_B)}{r_B} \chi_{-\kappa \mu_a}(\mathbf{r}_B) \end{pmatrix}. \quad (44)$$

The \bar{p} - and \bar{q} -functions, which are the relativistic analogs of the modified Löwdin $\bar{\alpha}$ -functions, are defined by

$$\begin{cases} \bar{p}_{\kappa\mu_b}(b|r_A) = \sum_{m_b, m_s} C_{l_b m_b, \frac{1}{2} m_s}^{j_b \mu_b} C_{l m_b, \frac{1}{2} m_s}^{j \mu_b} \bar{\alpha}_{l m_b}(P_b, l_b|r_A) \\ \bar{q}_{\kappa\mu_b}(b|r_A) = \sum_{m_b, m_s} C_{\bar{l}_b m_b, \frac{1}{2} m_s}^{j_b \mu_b} C_{\bar{l} m_b, \frac{1}{2} m_s}^{j \mu_b} \bar{\alpha}_{\bar{l} m_b}(Q_b, \bar{l}_b|r_A), \end{cases} \quad (45)$$

where $\bar{l} = l - \text{sign}(\kappa)$. Functions $\bar{\alpha}_{l m_b}(P_b, l_b|r_A)$ and $\bar{\alpha}_{\bar{l} m_b}(Q_b, \bar{l}_b|r_A)$ are defined by equation (41), where the function $f_b(r)$ has to be replaced by the functions $P_b(r)$ and $Q_b(r)$, respectively. Functions $\bar{p}_{\kappa\mu_a}(a|r_B)$ and $\bar{q}_{\kappa\mu_a}(a|r_B)$ are defined similarly to equation (45), where indices A and b should be replaced by B and a , respectively.

Two-center overlap integrals

Let us consider two-center overlap integrals $S_{ab}^{(0)}$. Here and below symbol (0) means that the integral is considered in the local coordinate frame, where the z -axis is directed along internuclear axis $A-B$.

The integral $S_{ab}^{(0)}$ can be divided into two parts

$$S_{ab}^{(0)} = \langle a | b \rangle = \langle a | b \rangle_A + \langle a | b \rangle_B, \quad (46)$$

where the notations $\langle \rangle_A$ and $\langle \rangle_B$ mean the integration over the regions V_A and V_B , respectively (see Fig. 2). Using the reexpansions of the large and small components onto the center A (in the region V_A) and onto the center B (in the region V_B) we obtain

$$\begin{cases} \langle a | b \rangle_A = \delta_{\mu_a, \mu_b} \int_0^\infty dr \left[P_a(r) \cdot \bar{p}_{\kappa_a \mu_a}(b|r) + Q_a(r) \cdot \bar{q}_{\kappa_a \mu_a}(b|r) \right] \\ \langle a | b \rangle_B = (-1)^{l_b - l_a} \delta_{\mu_a, \mu_b} \int_0^\infty dr \left[P_b(r) \cdot \bar{p}_{\kappa_b \mu_a}(a|r) + Q_b(r) \cdot \bar{q}_{\kappa_b \mu_a}(a|r) \right]. \end{cases} \quad (47)$$

Matrix elements of the nuclear attraction potentials, $V_{\text{nucl}}^A(r_A)$ and $V_{\text{nucl}}^B(r_B)$, and of the mass operator βmc^2 are calculated similarly to the overlap integral.

Two-center gradient matrix elements

As in case of the overlap integral, the region of integration for the gradient matrix element $G_{ab}^{(0)}(q)$ is divided into two parts,

$$G_{ab}^{(0)}(q) = \langle a | \nabla_q | b \rangle = \langle a | \nabla_q | b \rangle_A + \langle a | \nabla_q | b \rangle_B. \quad (48)$$

Here index $q = 1, 0, -1$ enumerates covariant spherical coordinates. Using the Gauss theorem [75] for the integration over region A , we obtain

$$G_{ab}^{(0)}(q) = -\langle b | \nabla_q | a \rangle_A + \langle a | \nabla_q | b \rangle_B + \delta_{q,0} \langle a | b \rangle_S, \quad (49)$$

where $\langle a | b \rangle_S$ is the surface integral over the region S (see Fig. 2). The volume integrals over regions A and B are given by

$$\begin{aligned} \langle b | \nabla_q | a \rangle_A &= \sum'_{\kappa} g^{1q}(j\mu_b, j_a\mu_a) \int_0^{\infty} dr \left[\bar{p}_{\kappa\mu_b}(b|r) \hat{D}_{\kappa,\kappa_a} P_a(r) + \bar{q}_{\kappa\mu_b}(b|r) \hat{D}_{-\kappa,-\kappa_a} Q_a(r) \right], \\ \langle a | \nabla_q | b \rangle_B &= \sum'_{\kappa} (-1)^{l_a-l} g^{1q}(j\mu_a, j_b\mu_b) \int_0^{\infty} dr \left[\bar{p}_{\kappa\mu_a}(a|r) \hat{D}_{\kappa,\kappa_b} P_b(r) + \bar{q}_{\kappa\mu_a}(a|r) \hat{D}_{-\kappa,-\kappa_b} Q_b(r) \right], \end{aligned} \quad (50)$$

where the prime at the sum symbol indicates that the summation is restricted to odd values of $l_a + l$ and $l_b + l$, and the operator $D_{\kappa,\kappa'}$ is defined by

$$D_{\kappa,\kappa'} = \frac{d}{dr} + \frac{\kappa'(\kappa' + 1) - \kappa(\kappa + 1)}{2r}. \quad (51)$$

The coefficients $g^{kq}(j\mu, j'\mu')$ are the relativistic analogs of the Gaunt coefficients [76]

$$g^{kq}(j\mu, j'\mu') = \frac{\sqrt{(2j+1)(2j'+1)}}{2k+1} (-1)^{\frac{1}{2}+\mu'} C_{j-\frac{1}{2},j'-\frac{1}{2}}^{k0} C_{j\mu,j'-\mu'}^{kq}. \quad (52)$$

The relativistic Gaunt coefficient is non-zero only if $l + l' + k$ is even.

The surface integral is given by

$$\begin{aligned} \langle a | b \rangle_S &= \delta_{\mu_a,\mu_b} \frac{1}{2} \left[\sum_{m,m_s} C_{l_a m, \frac{1}{2} m_s}^{j_a \mu_a} C_{l_b m, \frac{1}{2} m_s}^{j_b \mu_a} \int_{R/2}^{\infty} dr \frac{1}{r} P_a(r) P_b(r) U_{l_a l_b m} \left(\frac{R}{2r} \right) \right. \\ &\quad \times \left. \sum_{m,m_s} C_{l_a m, \frac{1}{2} m_s}^{j_a \mu_a} C_{l_b m, \frac{1}{2} m_s}^{j_b \mu_a} \int_{R/2}^{\infty} dr \frac{1}{r} Q_a(r) Q_b(r) U_{l_a l_b m} \left(\frac{R}{2r} \right) \right], \end{aligned} \quad (53)$$

where

$$U_{l_a, l_b, m}(x) = (-1)^{l_b-m} \sqrt{(2l_a+1)(2l_b+1)} K_{l_a|m|} K_{l_b|m|} P_{l_a}^{|m|}(x) P_{l_b}^{|m|}(x). \quad (54)$$

Two-center $(\boldsymbol{\alpha} \cdot \mathbf{p})$ matrix elements

Two-center $(\boldsymbol{\alpha} \cdot \mathbf{p})$ matrix elements $A_{ab}^{(0)}$ can be divided into three parts, similarly to the gradient matrix elements $G_{ab}^{(0)}(q)$ (49),

$$A_{ab}^{(0)} = \langle a | \boldsymbol{\alpha} \cdot \mathbf{p} | b \rangle = \langle b | \boldsymbol{\alpha} \cdot \mathbf{p} | a \rangle_A + \langle a | \boldsymbol{\alpha} \cdot \mathbf{p} | b \rangle_B + \frac{1}{i} \langle a | \boldsymbol{\alpha}_0 | b \rangle_S, \quad (55)$$

where the volume integrals $\langle b | \boldsymbol{\alpha} \cdot \mathbf{p} | a \rangle_A$ and $\langle b | \boldsymbol{\alpha} \cdot \mathbf{p} | a \rangle_A$ are given by

$$\begin{aligned} \langle b | \boldsymbol{\alpha} \cdot \mathbf{p} | a \rangle_A &= \delta_{\mu_a, \mu_b} \int_0^\infty dr \left[\left(-\frac{dQ_a}{dr} + \frac{\kappa_a Q_a}{r} \right) \bar{p}_{\kappa_a \mu_a}(b|r) + \left(\frac{dP_a}{dr} + \frac{\kappa_a P_a}{r} \right) \bar{q}_{\kappa_a \mu_a}(b|r) \right], \\ \langle a | \boldsymbol{\alpha} \cdot \mathbf{p} | b \rangle_B &= (-1)^{l_a - l_b} \delta_{\mu_a, \mu_b} \int_0^\infty dr \left[\left(-\frac{dQ_b}{dr} + \frac{\kappa_b Q_b}{r} \right) \bar{p}_{\kappa_b \mu_b}(a|r) + \left(\frac{dP_b}{dr} + \frac{\kappa_b P_b}{r} \right) \bar{q}_{\kappa_b \mu_b}(a|r) \right]. \end{aligned} \quad (56)$$

The last term in equation (55) is the surface integral, which is given by

$$\begin{aligned} \frac{1}{i} \langle a | \boldsymbol{\alpha}_0 | b \rangle_S &= \delta_{\mu_a, \mu_b} \sum_{m, m_s} m_s C_{\bar{l}_a m, \frac{1}{2} m_s}^{j_a \mu_a} C_{\bar{l}_b m, \frac{1}{2} m_s}^{j_b \mu_a} \int_{R/2}^\infty dr \frac{1}{r} Q_a(r) P_b(r) U_{\bar{l}_a \bar{l}_b m}(R/2r) \\ &+ \delta_{\mu_a, \mu_b} \sum_{m, m_s} m_s C_{\bar{l}_a m, \frac{1}{2} m_s}^{j_a \mu_a} C_{\bar{l}_b m, \frac{1}{2} m_s}^{j_b \mu_a} \int_{R/2}^\infty dr \frac{1}{r} P_a(r) Q_b(r) U_{\bar{l}_a \bar{l}_b m}(R/2r). \end{aligned} \quad (57)$$

Transformation of the two-center matrix elements to the laboratory frame

As indicated above, the laboratory frame S is defined to be at rest with respect to the initial target position. Then, the two-center matrix elements calculated in the local coordinate frame $S' = (x', y', z')$ (see Fig. 1) have to be transformed to the laboratory frame $S = (x, y, z)$. The corresponding two-center integrals can be obtained from $S_{ab}^{(0)}$, $H_{ab}^{(0)}$, and $G_{ab}^{(0)}$ by rotating the coordinate system around the y -axis for angle $-\theta$ (Fig. 1). For the overlap integrals S_{ab} and the two-center Dirac-Hamiltonian matrix elements H_{ab} in the laboratory frame S we obtain

$$\begin{aligned} S_{a,b} &= S_{n_a \kappa_a \mu_a; n_b \kappa_b \mu_b} = \sum_{\mu} d_{\mu_a \mu}^{j_a}(\theta) d_{\mu_b \mu}^{j_b*}(\theta) S_{n_a \kappa_a \mu; n_b \kappa_b \mu}^{(0)}, \\ H_{a,b} &= H_{n_a \kappa_a \mu_a; n_b \kappa_b \mu_b} = \sum_{\mu} d_{\mu_a \mu}^{j_a}(\theta) d_{\mu_b \mu}^{j_b*}(\theta) H_{n_a \kappa_a \mu; n_b \kappa_b \mu}^{(0)}, \end{aligned} \quad (58)$$

where $d_{\mu'\mu}^j(\theta)$ are real Wigner's D-functions [74]. The transformation of the gradient matrix elements $G_{ab}^{(0)}(q)$ to the laboratory frame S is given by

$$G_{ab}(q) = G_{n_a\kappa_a\mu_a; n_b\kappa_b\mu_b}(q) = \sum_{\mu'_a, \mu'_b, q} d_{\mu_a\mu'_a}^{j_a}(\theta) d_{\mu_b\mu'_b}^{j_b}(\theta) d_{q'q}^1(\theta) G_{n_a\kappa_a\mu'_a; n_b\kappa_b\mu'_b}^{(0)}(q). \quad (59)$$

D. Charge-transfer probabilities and cross sections

1. Transition amplitudes

Transition amplitude for electron capture to an ion state αn is given by

$$T_{\alpha n}(t) = \langle \psi_{\alpha n}(\mathbf{r}, t) | \Psi(\mathbf{r}, t) \rangle, \quad t \rightarrow \infty. \quad (60)$$

As previously mentioned, here index $\alpha = A, B$ enumerates different centers (target and projectile ions) and $\psi_{\alpha n}(\mathbf{r}, t)$ are the wave functions of the free-moving ion α . After the collision ($t \rightarrow \infty$) the wave functions $\psi_{\alpha n}(\mathbf{r}, t)$ of the free-moving ion α are given by

$$\psi_{\alpha n}(\mathbf{r}, t) = e^{-iE_{\alpha n}t} s_{\alpha}(\mathbf{r}) \psi_{\alpha n}^0(\mathbf{r} - \mathbf{R}_{\alpha}), \quad (61)$$

where $\psi_{\alpha n}^0(\mathbf{r})$ are the stationary Dirac wave functions of ion α at the rest and $s_{\alpha}(\mathbf{r})$ is the translation factor. For the low-energy collisions the translation factor and the energy $E_{\alpha n}$ of the moving ion can be taken in the nonrelativistic approximation

$$s_{\alpha}(\mathbf{r}) = \exp(i\mathbf{v}_{\alpha} \cdot \mathbf{r}), \quad E_{\alpha n} = \varepsilon_{\alpha n} + v_{\alpha}^2/2. \quad (62)$$

Generally, the translation factor is introduced in the basis functions to improve the convergence of the time-dependent wave function expansion. We did not include the translation factor $s_{\alpha}(\mathbf{r})$ in the basis functions because of the computational complexity of the two-center integral calculations. However, at the limit $t \rightarrow \infty$ we can reexpand the moving orbitals $s_{\alpha}\varphi_{\alpha n}$ over the basis $\varphi_{\alpha n}$ in the following way. At the limit $t \rightarrow \infty$ the basis functions of the different centers do not overlap. The basis set φ_j is orthonormal and

$$e^{-i\mathbf{v}_{\alpha} \cdot \mathbf{r}} \varphi_{\alpha n}(\mathbf{r}) \simeq \sum_{n'} K_{\alpha n', \alpha n} \varphi_{\alpha n'}(\mathbf{r}), \quad K_{\alpha n', \alpha n} = \delta_{\alpha, \alpha'} \langle \varphi_{\alpha n'} | e^{-i\mathbf{v}_{\alpha} \cdot \mathbf{r}} | \varphi_{\alpha n} \rangle. \quad (63)$$

The expansion (63) is not exact, since the finite basis $\varphi_{\alpha n}$ is incomplete and K is non-unitary matrix. In particular,

$$\sum_{n'} |K_{\alpha n', \alpha n}|^2 < 1. \quad (64)$$

We can renormalize matrix K and rewrite expansion (63) in the form

$$e^{-i\mathbf{v}_\alpha \cdot \mathbf{r}} \varphi_{\alpha n}(\mathbf{r}) \simeq \sum_{n'} \bar{K}_{\alpha n', \alpha n} \varphi_{\alpha n'}(\mathbf{r}), \quad \bar{K} = N K, \quad N = (K K^+)^{-1/2}. \quad (65)$$

Here matrix N plays a role of the normalization factor. The renormalized matrix \bar{K} is unitary.

Now we can obtain the expansion of the time-dependent wave function $\Psi(\mathbf{r}, t)$ over the basis functions with translation factor ($t \rightarrow \infty$),

$$\Psi(\mathbf{r}, t) = \sum_{\alpha, n} C_{\alpha n}(t) \varphi_{\alpha, n}(\mathbf{r}) \simeq \sum_{\alpha, n} \bar{C}_{\alpha n}(t) e^{i\mathbf{v}_\alpha \cdot \mathbf{r}} \varphi_{\alpha n}(\mathbf{r}), \quad (66)$$

where

$$\bar{C}_{\alpha n}(t) = \sum_{n'} \bar{K}_{\alpha n, \alpha n'} C_{\alpha n'}(t). \quad (67)$$

It should be noted that the set of coefficients $\bar{C}_{\alpha n}(t)$ is normalized to unity

$$\sum_{\alpha, n} |\bar{C}_{\alpha n}(t)|^2 = \sum_{\alpha, n} |C_{\alpha n}(t)|^2 = 1, \quad t \rightarrow \infty. \quad (68)$$

Therefore, for the transition amplitude $T_{\alpha n}(t)$ we obtain

$$T_{\alpha n}(t) = \langle \psi_{\alpha n}(\mathbf{r}, t) | \Psi(\mathbf{r}, t) \rangle = \sum_{n'} \bar{C}_{\alpha n'}(t) e^{iE_{\alpha n} t} \langle \psi_{\alpha n}^0 | \varphi_{\alpha n'} \rangle, \quad t \rightarrow \infty. \quad (69)$$

The stationary Dirac wave functions $\psi_{\alpha n}^0$, including wave functions of the positive and negative energy spectra, form a complete basis set. Therefore,

$$\sum_{\alpha, n} |T_{\alpha n}|^2 = \sum_{\alpha, n} |\bar{C}_{\alpha n}(t)|^2 = 1. \quad (70)$$

2. Transition probabilities

Transition probabilities $W_{\alpha n}(t)$ are defined by

$$W_{\alpha n}(t) = |T_{\alpha n}(t)|^2. \quad (71)$$

The probability $W_{\alpha n}(t)$, defined by equations (71) and (69), has an oscillatory behavior at $t \rightarrow \infty$, because the basis functions $\varphi_{\alpha, n}$ are not the solutions of the hydrogen-like Dirac equation and the basis set is truncated. We can remove the oscillatory component of the probability $W_{\alpha n}(t)$ for the large time ($t \rightarrow \infty$) in the same way, as it was done in Refs. [7, 8].

At the large time ($t \rightarrow \infty$) the coefficients $C_j^L(t)$ coincide with the coefficients $C_j(t)$. Therefore, the coefficients $C_j(t)$ are the solutions of equation (17)

$$i \frac{d\mathbf{C}(t)}{dt} = M(t) \mathbf{C}(t). \quad (72)$$

Then for the coefficients $\overline{C}_j(t)$ we obtain the equation

$$i \frac{d\overline{\mathbf{C}}(t)}{dt} = \overline{K} M(t) \overline{K}^+ \overline{\mathbf{C}}(t). \quad (73)$$

Using the diagonalization procedure for the Hermitian matrix $\overline{K} M \overline{K}^+$, we can decompose

$$\overline{K} M \overline{K}^+ = V \Omega V^+, \quad (74)$$

where Ω is a diagonal matrix with eigenvalues $\Omega_{kk} = \omega_k$ and V is a unitary matrix.

We introduce new coefficients $\mathbf{B}(t)$ by

$$B_k(t) = \left(e^{i\Omega t} V^+ \overline{\mathbf{C}}(t) \right)_k = e^{i\omega_k t} \sum_j V_{jk}^* \overline{C}_j(t), \quad \sum_k |B_k(t)|^2 = 1. \quad (75)$$

These coefficients have well defined limits at $t \rightarrow \infty$. The amplitudes $T_{\alpha n}(t)$, defined by equation (69), in terms of the coefficients $\mathbf{B}(t)$ are given by

$$T_j(t) = \sum_{k,l} e^{i(E_j - \omega_k)t} V_{lk} B_k \langle \psi_j^0 | \varphi_l \rangle. \quad (76)$$

Then for the probabilities $W_j(t)$ we obtain

$$W_j(t) = |T_j(t)|^2 = \sum_k |B_k(t)|^2 \left| \sum_l V_{lk} \langle \psi_j^0 | \varphi_l \rangle \right|^2 + (\text{oscillating term}). \quad (77)$$

Removing the oscillating term [8], we can introduce probabilities $W'_j(t)$ defined as

$$W'_j(t) = \sum_k |B_k(t)|^2 \left| \sum_l V_{lk} \langle \psi_j^0 | \varphi_l \rangle \right|^2. \quad (78)$$

Since hydrogen-like Dirac wave functions $\psi_{\alpha,n}^0$ of each center α (including the positive and negative Dirac continuum spectra) form a complete basis set, we get

$$\sum_{j \in \alpha} |W'_j(t)|^2 = \sum_k |B(k)|^2 \sum_l |V_{kl}|^2 = \sum_k |B(k)|^2 = 1. \quad (79)$$

The coefficients $B_k(t)$ and the matrix elements have well-defined limits for $t \rightarrow \infty$. Therefore, there exists the limit

$$P_{\alpha,n} = \lim_{t \rightarrow \infty} W'_{\alpha n}(t). \quad (80)$$

The direct (P_d), charge transfer (P_{ct}), and ionization (P_{ion}) probabilities are given by

$$P_d = \sum'_n P_{A,n}, \quad P_{ct} = \sum'_n P_{B,n}, \quad P_{ion} = 1 - \sum'_{\alpha,n} P_{\alpha n} = 1 - P_d - P_{ct}. \quad (81)$$

where the prime at the sum symbol indicates that the summation runs over the discrete bound states of the ion α .

The cross sections for the charge transfer (σ_{ct}) and ionization (σ_{ion}) processes are then calculated as usual by integrating the probabilities over the impact parameter b :

$$\sigma_{ct} = 2\pi \int_0^\infty db \, b \, P_{ct}(b), \quad \sigma_{ion} = 2\pi \int_0^\infty db \, b \, P_{ion}(b). \quad (82)$$

3. *Z-scaling*

It is well-known that in the nonrelativistic theory the scale transformation $\mathbf{r}' = Z \mathbf{r}$ and $R' = Z R$ allows one to transform the wave functions $\psi(\mathbf{r})$ and the energies ε of a homonuclear one-electron quasi-molecule with a point nuclear charge $Z > 1$ to the wave functions $\psi'(\mathbf{r}) = Z^{-3/2} \psi(Z \mathbf{r})$ and energies $\varepsilon' = \varepsilon/Z^2$ of the H_2^+ molecule. The same scale transformation can be considered in the nonrelativistic homonuclear collisions.

The time-dependent Schrödinger equation describing $A^{(Z-1)+}-A^{Z+}$ collision is given by

$$\left(-\frac{1}{2} \Delta + \frac{Z}{|\mathbf{r} - \mathbf{R}_A(t)|} + \frac{Z}{|\mathbf{r} - \mathbf{R}_B(t)|} \right) \Psi(\mathbf{r}, t) = i \frac{\partial}{\partial t} \Psi(\mathbf{r}, t). \quad (83)$$

If in Eq. (83) we set $\mathbf{r}' = Z \mathbf{r}$, $t' = Z^2 t$, and $\mathbf{R}'_\alpha(t') = Z \mathbf{R}_\alpha(t)$, we obtain the time-dependent Schrödinger equation for the H^+-H collision [4, 19]

$$\left(-\frac{1}{2} \Delta' + \frac{1}{|\mathbf{r}' - \mathbf{R}'_A(t')|} + \frac{1}{|\mathbf{r}' - \mathbf{R}'_B(t')|} \right) \Psi(\mathbf{r}', t') = i \frac{\partial}{\partial t'} \Psi(\mathbf{r}', t'). \quad (84)$$

It should be noted that the scaling $R' = ZR(t)$ is satisfied exactly for a straight-line trajectory. In this case the impact parameter b , the velocity v_α , and projectile energy E are transformed by

$$b' = Zb, \quad v'_\alpha = v_\alpha/Z, \quad E' = E/Z^2. \quad (85)$$

It follows that the probability $P_{\alpha,n}(Z, b, E)$ and the cross section $\sigma_{\alpha,n}(Z, E)$ for a process in a symmetric system with nuclei of charge Z can be obtained from the probability $P_{\alpha,n}(1, b', E')$ and the cross section $\sigma_{\alpha,n}(1, E')$ for the same process in the $H(1s)-H^+$ system by the relations

$$P_{\alpha,n}(Z, b, E) = P_{\alpha,n}(1, bZ, E/Z^2), \quad \sigma_{\alpha,n}(Z, E) = \frac{1}{Z^2} \sigma_{\alpha,n}(1, E/Z^2). \quad (86)$$

It should be noted that this scaling law is not valid for the relativistic collisions.

III. RESULTS

A. The choice of the basis

In our relativistic calculations, we used two Dirac-Sturm bases of different size. Both bases include functions of the positive-energy Dirac spectrum and Sturm orbitals corresponding to the negative-energy Dirac spectrum. It should be noted that the constructed bases satisfy the dual kinetic balance conditions [77] and do not contain so-called “spurious” states [78].

The positive-energy functions of the first basis (Basis 1) on each center in the standard nonrelativistic notations of atomic shells are given by: $1s-3s$, $2p, 3p$, $3d$, $\overline{4s}-\overline{6s}$, $\overline{4p}-\overline{6p}$, $\overline{4d}-\overline{6d}$, $\overline{4f}, \overline{5f}$. Here the overline symbol (\overline{nl}) is used to indicate the Dirac-Sturm (pseudo-state) basis functions. The total number of the positive-energy orbitals of both centers is 220 and the total size of Basis 1, including the negative-energy orbitals, is 440. Basis 1 is used for both stationary and time-dependent wave functions.

The basis size can be increased in the calculations of the stationary states of quasi-molecules. Positive-energy functions of the second basis (Basis 2) is constructed from 26 atomic shells: $1s$, $\overline{2s}-\overline{8s}$, $\overline{2p}-\overline{8p}$, $\overline{3d}-\overline{8d}$, $\overline{4f}-\overline{6f}$, $\overline{5g}, \overline{6g}$. In Basis 2, the total number of orbitals of both ions, including the negative-energy spectrum, is equal to 784. This basis is used only in the calculations of the stationary states of quasi-molecules.

B. Stationary ground states of some homonuclear quasi-molecules

1. Energies of the ground state of some homonuclear quasi-molecules

In Table I we present the results of our relativistic calculations of the $1\sigma_g$ state energy of the H_2^+ , Th_2^{179+} , and U_2^{183+} quasi-molecules for so-called chemical distance $R = 2/Z$ a.u.. Since the quasi-molecule Th_2^{179+} was considered as a reference system for testing relativistic effects, it was calculated in a number of papers using high-precision large-scale methods (see, e.g., Refs. [59, 79–81]). As one

TABLE I: Relativistic energies (a.u.) of the $1\sigma_g$ state of quasi-molecules for the point-charge nuclei and $R = 2/Z$ a.u..

	$\text{H}_2^+ (Z = 1)$		$\text{Th}_2^{179+} (Z = 90)$		$\text{U}_2^{183+} (Z = 92)$
	$\epsilon_{1\sigma_+}$	Rel. error	$\epsilon_{1\sigma_+}$	Rel. error	$\epsilon_{1\sigma_+}$
Basis 1	−1.1026248	$1.5 \cdot 10^{-5}$	−9504.573	$1.9 \cdot 10^{-5}$	−9965.190
Basis 2	−1.1026405	$1.0 \cdot 10^{-6}$	−9504.732	$2.5 \cdot 10^{-6}$	−9965.307
Others	−1.1026416 ^a		−9504.756 ^b		

^a Ref. [58]

^b Ref. [59]

can seen from Table I, there is a good agreement of our data with very accurate values obtained in Refs. [58, 59]. The relative precision of our results for the quasi-molecules H_2^+ and Th_2^{179+} is increased by an order of magnitude when Basis 1 is replaced by Basis 2.

In Fig. 3 we display the energy of the $1\sigma_g$ state of the U_2^{183+} quasi-molecule as a function of the internuclear distance R on a logarithmic scale. In this figure the solid line indicates the energy $E(R)$ calculated using two-center Dirac-Sturm Basis 2. The dashed line represent the results of the one-center calculations in the monopole approximation. As one can see from Fig. 3, in the two-center basis the $1\sigma_g$ electron ”dives” into the negative-energy Dirac continuum at a critical distance $R_c = 34.7$ fm. The critical distance obtained in our monopole approximation amounts to $R_c = 25.5$ fm that is too far from the exact value. It should be noted that in our one-center monopole approximation the basis was

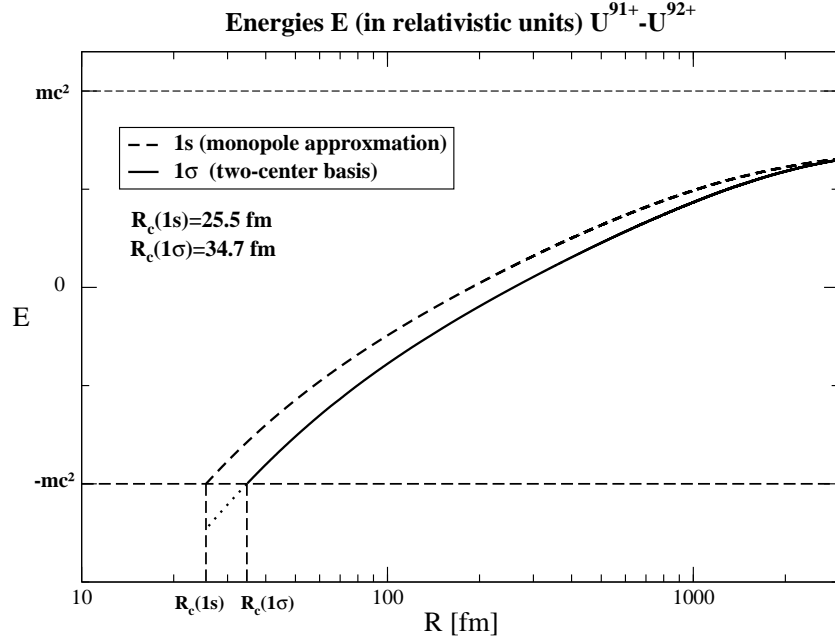


FIG. 3: The $1\sigma_g$ state energy of the U_2 quasi-molecule as a function of the internuclear distance R on a logarithmic scale.

centered at the position of the nucleus (A or B) but not at the center of the internuclear interval, as it was done in the papers [41, 62, 82]. The monopole approximation used in Ref. [41] is more suitable for the short-distance regime and gives the value of the critical distance equal to $R_c = 35$ fm.

2. Critical distance

In the Table II we present our results of the two-center relativistic calculations (Basis 2) of the critical distance R_c for homonuclear one-electron quasi-molecules $A_2^{(2Z-1)+}$ and compare them with the corresponding values obtained by other authors. There exists a discrepancy of about 5-10% between the critical distance data for the point nuclei [27, 41, 60, 61, 83, 84]. Our results for this case are in a very good agreement with the results of Ref. [60]. In our calculations for extended nuclei, the finite nuclear size was taken into account using the Fermi model of the nuclear charge distribution (for details, see, e.g., Ref. [85]). The root-mean-square nuclear charge radii $\langle R_n^2 \rangle^{1/2}$ were taken from Refs. [86] (for $Z=88$), [87] (for $Z=90$), [88] (for $Z=92$), and [89] (for $Z=94, 96, 98$). The number of works where the finite nuclear size effect was taken into account is much less than for the point nucleus case. We can systematically compare our results only with the data obtained in Ref. [63]. The discrepancy

TABLE II: Critical distances R_c (fm) for homonuclear one-electron quasi-molecules $A_2^{(2Z-1)+}$.

Z	Point nucleus		Extended nucleus		
	This work	Others	$\langle R_n^2 \rangle^{1/2}(\text{fm})$	This work	Others
88	24.27	24.24 ^a	5.5705	19.91	19.4 ^c
90	30.96	30.96 ^a	5.7210	27.05	26.5 ^c
92	38.43	38.42 ^a 36.8 ^b	5.8569	34.72	34.3 ^c 34.7 ^d
94	46.58	46.57 ^a	5.794	43.16	42.6 ^c
96	55.38	55.37 ^a	5.816	52.09	51.6 ^c
98	64.79	64.79 ^a	5.844	61.63	61.0 ^c 61.1 ^d

^a Ref. [60], ^b Ref. [27], ^c Ref. [63], ^d Ref. [62]

between our data and those from Ref. [63] is considerably larger for the extended nuclei than for the point nuclei. A possible reason of that could consist in a rather crude estimate of the nuclear size effect in Ref. [63]. It should also be noted that in the work [63] other values of the nuclear radii, namely $\langle R_n^2 \rangle^{1/2} = \sqrt{3/5} \cdot 1.2 \cdot (2.6 \cdot Z)^{1/3}$ were used. Our calculations showed, however, that the usage of the nuclear radii from Ref. [63] changes the values of R_{cr} not more than by 0.02 fm.

C. Charge-transfer probabilities and cross sections

1. $H(1s)-H^+$ collisions

Fig. 4 shows the charge-transfer probabilities $P_{ct}(b)$ for the $H(1s)-H^+$ collision as functions of the impact parameter b for the projectile energies of 2 keV and 5 keV. The results of our relativistic calculations for 2 keV (solid line) and 5 keV (dashed line) are found to be very close to nonrelativistic calculations based on the two-center atomic-orbital (AO) expansion [5, 90]. This is not surprising, since the relativistic effects are negligible for the $H(1s)-H^+$ collision. Our calculations were performed for the straight-line trajectory of the projectile that corresponds to the full screening of the target nuclear

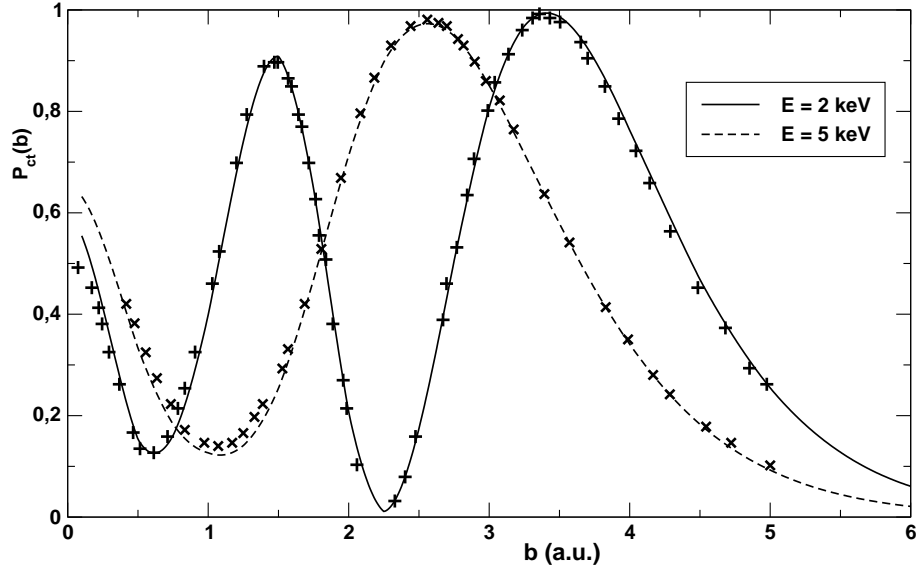


FIG. 4: Charge-transfer probabilities $P_{\text{ch}}(b)$ for the $\text{H}(1s)\text{-H}^+$ collision as functions of the impact parameter b . Our results for the projectile energies 2 keV (solid line) and 5 keV (dashed line) are compared to the related results from the AO-expansion calculations [5, 90] (symbols “+” and “x”).

charge by the $1s$ -electron.

As was demonstrated in Ref. [5], the two-center AO expansion data are in a very good agreement with results obtained by a direct numerical solution of the nonrelativistic Schrödinger equation [14]. In the review [5], the two-center AO expansion data [90] are also compared with the results [91, 92], obtained by the expansion over the “nonmoving” Hylleraas functions. It should be noted that the Hylleraas expansion data are similar to the results of Refs. [90], [14] and to our results in trend but differ by the phase and the magnitude.

In Table III we present the total charge-transfer cross sections σ_{ct} for the $\text{H}(1s)\text{-H}^+$ collision in a wide range of the projectile energy (from 0.5 keV to 100 keV) and compare them with nonrelativistic large-scale calculations of the recent paper [13], which can be considered as an extension of the pioneering works [8, 93], where the analytical Sturmian basis set expansion was used. We also give the cross section values, deduced from the experimental results [94]. The relative uncertainties of the recommended and interpolated experimental data are about 5%-10%. As one can see from the table III, our results are in a good agreement with the theoretical data of Ref. [13] and with the experimental data.

TABLE III: Charge transfer cross section σ_{ct} for the $H(1s)-H^+$ collision, in units of 10^{-17} cm^2 .

Projectile energy	$\sigma_{ct}(E)$	$\sigma_{ct}(E)$	$\sigma_{ct}(E)$
E (keV)	This work	Winter [13]	Exp ^a
0.5	199.6		
0.7	186.9		
1.0	172.4	173.0	171
2.0	144.9		144
4.0	117.5	118.1	115*
5.0	107.8		110
10.0	81.3		77.5
15.0	63.5	67.41	55.6*
20.0	48.9		44.5
25.0	36.2	39.45	35.3*
30.0	26.6		27.6*
40.0	15.3		16.5*
50.0	9.1	10.04	9.9
60.0	5.6		5.9*
70.0	3.5		3.6*
80.0	2.3		2.3*
100.0	1.1	1.11	1.1

^a Recommended values [94] deduced from the experimental data.

* Interpolated values obtained using an analytic fitting function [94].

The ionization cross sections, computed in this work using equations (81) and (82), are displayed in Fig. 5. Our results are in a good agreement with the experimental data in the range of the proton energy from 20 keV to 80 keV. At the energies less than 15 keV we observe a significant relative deviation of our results from the experimental data. Thus is probably due to the fact that the absolute uncertainty of our data is approximately the same in the whole region of the energies (about $(1-3) \cdot 10^{-17} \text{ cm}^2$), while at the low energies the ionization cross section tends to zero. This leads to a large relative error in the low energy region.

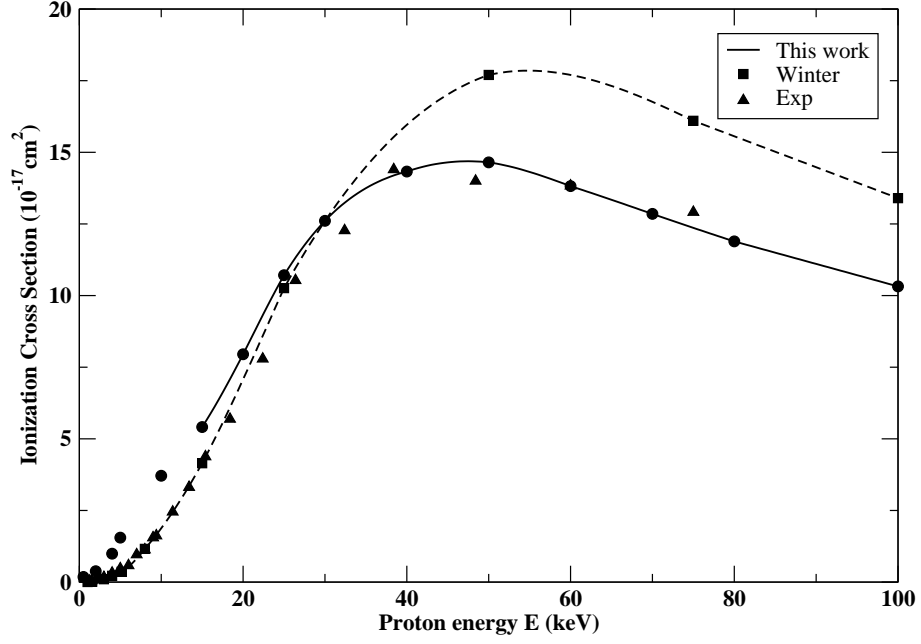


FIG. 5: Ionization cross section $\sigma_{\text{ion}}(E)$ for the $\text{H}(1s)\text{-H}^+$ collision as a function of the projectile energy E . The solid line is obtained by the interpolation of our results indicated by circles, the dashed line is obtained by the interpolation of data from Ref. [13], and the triangles indicate the experimental data from Refs. [95, 96].

In contrast to our results, the theoretical data of Ref. [13], which are shown in Fig. 5 by squares, are in a good agreement with the experimental data in the low energy region (less than 25 keV) and significantly differ (at least by 25%) from the experimental data for the energies larger than 40 keV. The reason of this discrepancy is unclear to us.

2. $\text{Ne}^{9+}(1s)\text{-Ne}^{10+}$ collisions

To study the role of the relativistic effects in the homonuclear collisions and to test our approach we calculated the charge transfer cross sections for the $\text{Ne}^{9+}(1s)\text{-Ne}^{10+}$ collisions with the standard value of the speed of light ($c = 137.036$ a.u.) and in the nonrelativistic limit ($c \rightarrow \infty$) by multiplying the standard value of the speed of light by the factor 1000. The obtained values are presented in Table IV. It should be noted that the projectile energy values are divided by Z^2 (Z is the nuclear charge) and the values of the ionization cross section σ_{ion} are multiplied by the factor Z^2 . This was done in order to compare the $\text{Ne}^{9+}(1s)\text{-Ne}^{10+}$ cross section data with the $\text{H}(1s)\text{-H}^+$ results in accordance with the

TABLE IV: Charge transfer cross section $\sigma_{\text{ct}}(E)$ (10^{-17} cm²) as a function of the projectile energy E for the $\text{Ne}^{9+}(1s)\text{-Ne}^{10+}$ ($Z=10$) and $\text{H}(1s)\text{-H}^+$ collisions.

	$\text{Ne}^{9+}(1s)\text{-Ne}^{10+}$		$\text{H}(1s)\text{-H}^+$	$\text{Ne}^{9+}(1s)\text{-Ne}^{10+}$
E/Z^2 (keV/u)	$\sigma_{\text{ct}}(E) \cdot Z^2$ Rel. ^a	$\sigma_{\text{ct}}(E) \cdot Z^2$ Nonrel. ^b	$\sigma_{\text{ct}}(E)$	$\sigma_{\text{ct}}(E) \cdot Z^2$ Born approximation ^c
1.0	171.6	172.2	172.4	188.4
2.0	144.3	144.8	144.9	150.7
4.0	117.1	117.5	117.5	114.8
5.0	107.3	107.7	107.8	107.3
10.0	80.8	81.3	81.3	76.2
15.0	63.0	63.5	63.5	57.6
20.0	48.5	48.9	48.9	48.2
25.0	35.9	36.2	36.2	38.1
30.0	26.4	26.7	26.6	30.1
40.0	15.1	15.3	15.3	19.9
50.0	9.0	9.1	9.1	13.7
60.0	5.6	5.6	5.6	9.1
70.0	3.5	3.5	3.5	5.4
80.0	2.3	2.3	2.3	3.6
100.0	1.1	1.1	1.1	2.0

^a Relativistic calculations.

^b Nonrelativistic limit ($c \rightarrow \infty$).

^c Born approximation [97].

scaling low (86). As one can see from the table, the relativistic effects, which decrease the values of the charge-transfer cross section, are rather small and can be estimated as $0.5\text{-}0.8 (\alpha Z)^2$, where α is the fine-structure constant. In Table IV, we also compare our scaled nonrelativistic $\text{Ne}^{9+}(1s)\text{-Ne}^{10+}$ data with the $\text{H}(1s)\text{-H}^+$ results. It should be noted that our calculations for the $\text{Ne}^{9+}(1s)\text{-Ne}^{10+}$ collision were performed for the Rutherford trajectory (see section II A 2). This is probably the reason of a very small discrepancy between the data presented in the 3-rd and 4-th columns of Table IV.

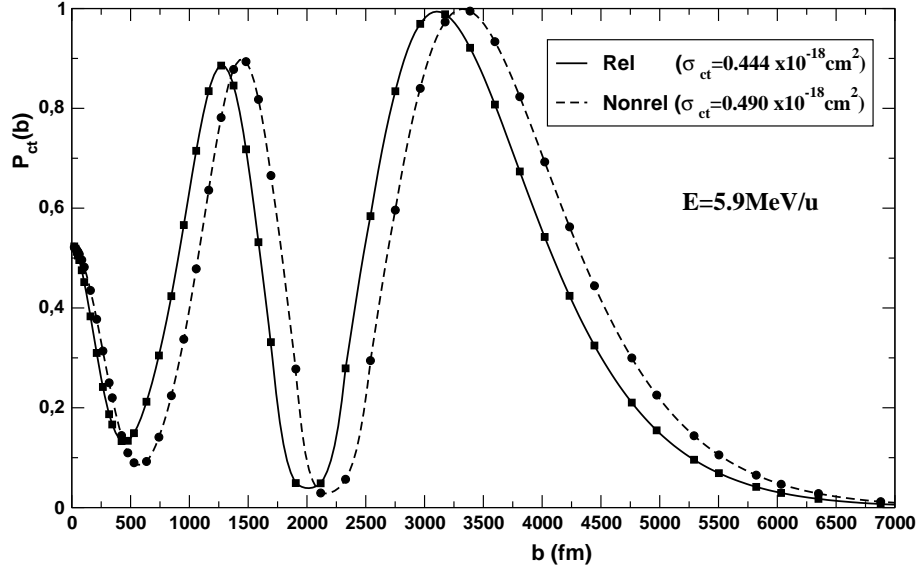


FIG. 6: The charge-transfer probability $P_{\text{ch}}(b)$ for the $\text{Xe}^{53+}(1s)\text{-Xe}^{54+}$ collision as a function of the impact parameter b . The solid line interpolates the relativistic values (squares) and the dashed line corresponds to the nonrelativistic limit. In both cases, the projectile energy is $E=5.9$ MeV/u.

It is also of interest to compare our results with the calculations performed within the plane wave Born (PWB) approximation. The results of such a calculation for the $\text{Ne}^{9+}(1s)\text{-Ne}^{10+}$ collision [97] are presented in the 5-th column of Table IV. The details of the modified PWB method can be found in Ref. [98]. It is seen from the table, that the PWB data are in a reasonable agreement with the more elaborated calculation.

3. $\text{Xe}^{53+}(1s)\text{-Xe}^{54+}$ collisions

The relativistic effect for the $\text{Xe}^{53+}(1s)\text{-Xe}^{54+}$ collisions is considerably larger than for the $\text{Ne}^{9+}(1s)\text{-Ne}^{10+}$ collisions. The computed relativistic (solid line) and nonrelativistic (dashed line) charge transfer probabilities $P_{\text{ct}}(b)$ as functions of the impact parameter b for the projectile energy of 5.9 MeV/u are displayed in Fig. 6. The oscillatory behavior of both curves is the same but the nonrelativistic curve is shifted toward higher energies.

In Table V we present the relativistic and non-relativistic values of the charge-transfer cross section for the $\text{Xe}^{53+}(1s)\text{-Xe}^{54+}$ collision scaled to $Z = 1$. One can see from the table, the relativistic effect

increases from 10% to 40% with increasing the projectile energy.

TABLE V: The charge transfer cross section $\sigma_{\text{ct}}(E)$ (10^{-17} cm²) as a function of the projectile energy E for the $\text{Xe}^{9+}(1s)\text{-Xe}^{10+}$ and $\text{H}(1s)\text{-H}^+$ collisions.

		$\text{Xe}^{53+}(1s)\text{-Xe}^{54+}$ ($Z=54$)		$\text{H}(1s)\text{-H}^+$ ($Z=1$)
E/Z^2 (keV/u)	E (MeV/u)	$\sigma_{\text{ct}}(E) \cdot Z^2$ Rel. ^a	$\sigma_{\text{ct}}(E) \cdot Z^2$ Nonrel. ^b	$\sigma_{\text{ct}}(E)$
1.23457	3.6	148.3	163.3	165.0
2.02332	5.9	129.4	143.0	144.9
3.42936	10.0	109.1	123.8	124.8
34.2936	100.0	13.3	20.6	20.7

^a Relativistic calculations.

^b Nonrelativistic limit ($c \rightarrow \infty$).

4. $\text{U}^{91+}(1s)\text{-U}^{92+}$ collisions

The calculations of the charge-transfer probabilities and cross sections for the $\text{U}^{91+}(1s)\text{-U}^{92+}$ collisions were performed for the extended nuclei. The Fermi model of the nuclear charge distribution with $R_{\text{nucl}} = 5.8569$ fm was used [88].

The computed relativistic (squares) and non-relativistic (circles) values of the charge-transfer probabilities $P_{\text{ct}}(b)$ and the interpolating curves are displayed in Fig. 7. It is seen from the figure, the nonrelativistic and relativistic probabilities significantly differ. The nonrelativistic curve (dashed line) is shifted toward higher energies compared to the relativistic one (solid line). The same curves in the small impact parameter region are shown in Fig. 8. In this figure, the vertical dashed line indicates the critical impact parameter $b_c = 27.5$ fm. For $b = b_c$ the $1\sigma_g$ ground state level of the U_2^{193+} quasi-molecule reaches the negative-energy Dirac continuum. It should be noted that for the non-straight-line (Rutherford) trajectory the value of the critical impact parameter b_c is less than the critical distance R_c presented in Table II. For values b smaller than b_c the $1\sigma_g$ level “dives” into the negative-energy continuum.

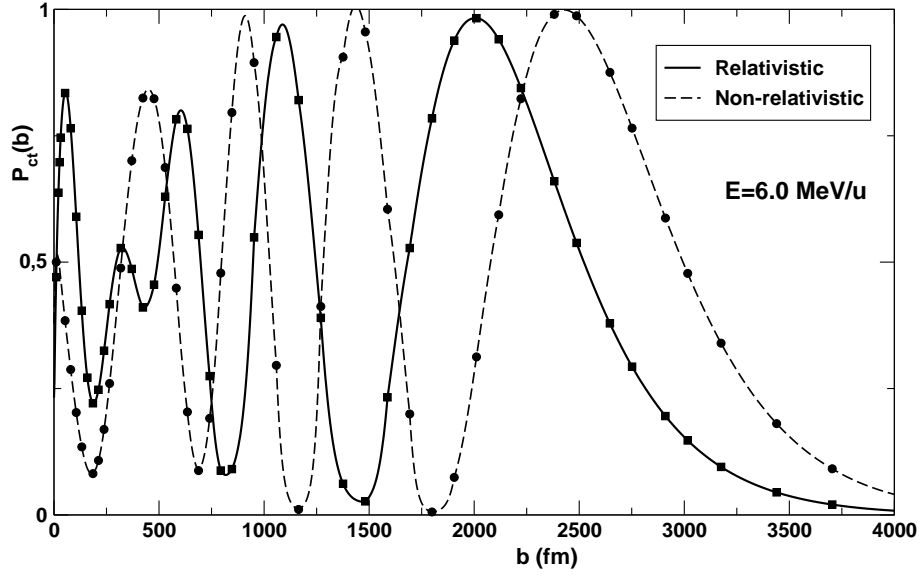


FIG. 7: Charge-transfer probability $P_{\text{ch}}(b)$ for the $\text{U}^{91+}(1s)\text{--}\text{U}^{92+}$ collision as a function of the impact parameter b . The solid line interpolates the relativistic values (squares) and the dashed line corresponds to the nonrelativistic limit. In both cases, the projectile energy is $E = 6.0$ MeV/u.

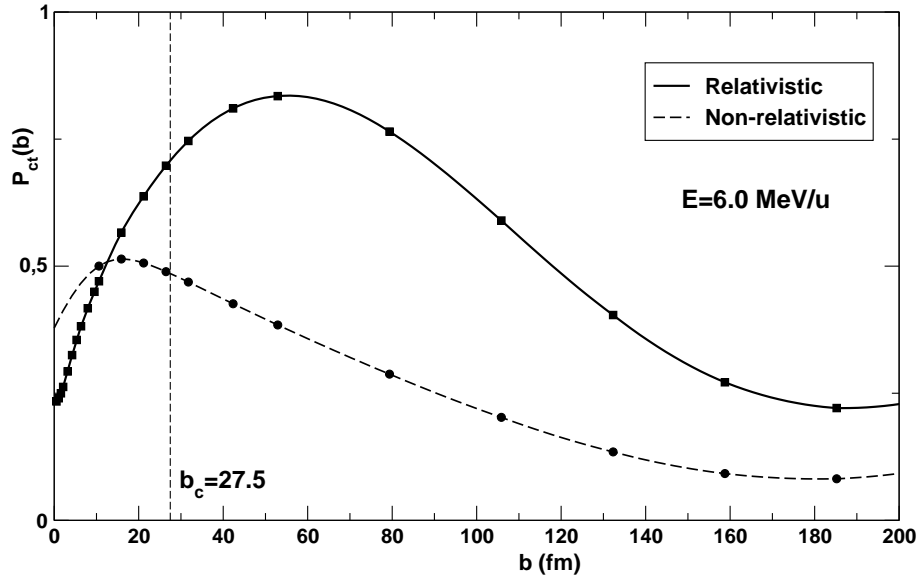


FIG. 8: Charge transfer probability $P_{\text{ct}}(b)$ for the $\text{U}^{91+}(1s)\text{--}\text{U}^{92+}$ collision as a function of the impact parameter b in the small b region. The value $b = b_c$ corresponds to the diving of the $1\sigma_g$ level into the negative-energy Dirac continuum. The solid line interpolates the relativistic values while the dashed line corresponds to the nonrelativistic limit.

In Table VI we present the results of our relativistic (3-rd column) and non-relativistic (4-th column) calculations of the total charge-transfer cross section $\sigma_{\text{ct}}(E)$, scaled to $Z = 1$, for the $\text{U}^{91+}(1s) - \text{U}^{92+}$ collision at different values of the projectile energy E . The values of $\sigma_{\text{ct}}(E)$ were obtained for the

TABLE VI: Charge transfer cross section $\sigma_{\text{ct}}(E)$ (10^{-17} cm^2) as a function of the projectile energy E for the $\text{U}^{91+}(1s)\text{-U}^{92+}$ and $\text{H}(1s)\text{-H}^+$ collisions.

	$\text{U}^{91+}(1s)\text{-U}^{92+}$				$\text{H}(1s)\text{-H}^+$
Energy E/Z^2 (keV/u)	Energy E (MeV/u)	$\sigma_{\text{ct}} \cdot Z^2$ Rel.	$\sigma_{\text{ct}} \cdot Z^2$ Nonrel.	$\sigma_{\text{ct}} \cdot Z^2$ Nonrel. str. line	σ_{ct}
0.70889	6.0	135.3	184.2	185.0	186.4
0.76796	6.5	132.7	181.3	182.0	183.1
0.82703	7.0	130.3	178.2	179.1	180.1
1.18147	10.0	117.1	165.8	166.7	167.6

Rutherford trajectories of the target and projectile ions. One can see from the table, the relativistic effect amounts to about 30% of the non-relativistic value of σ_{ct} . In the 5-th column of Table VI, we also present our results obtained for the straight-line trajectory of the projectile ion (in this case the target ion is at rest). As one can see from the table, the difference between the results obtained for the straight-line trajectory and the Rutherford one is very small. The non-relativistic values of the charge-transfer cross section for the $\text{U}^{91+}(1s)\text{-U}^{92+}$ collision, scaled to $Z = 1$, are also compared with the cross section $\sigma_{\text{ct}}(E)$ for the $\text{H}(1s)\text{-H}^+$ collision, presented in the 6-th column of Table VI.

IV. CONCLUSION

In this paper we presented a new method for the relativistic calculations of one-electron two-center quasi-molecular system in both stationary and time-dependent regimes. The method is suitable for a wide range of the internuclear distances including the critical regime, when the ground state of the quasi-molecule can dive into the negative-energy Dirac continuum. Using this method we calculated the energies of the H_2 , Th_2^{179+} and U_2^{183+} quasi-molecules, the critical distances for some homonuclear

quasi-molecules $A^{+(2Z-1)}$ ($Z=88, 90, 92, 94, 96, 98$), and the charge transfer probabilities, charge transfer and ionization cross sections for the $H(1s)-H^+$, $Ne^{9+}(1s)-Ne^{10+}$, $Xe^{53+}(1s)-Xe^{54+}$, and $U^{91+}(1s)-U^{92+}$ low-energy collisions.

The results of our calculations of the charge transfer probabilities and cross sections for the $H(1s)-H^+$ collision are in a good agreement with experimental data and with theoretical results obtained by other authors. The influence of the relativistic effect on the charge transfer probabilities and cross sections for the $Ne^{9+}(1s)-Ne^{10+}$, $Xe^{53+}(1s)-Xe^{54+}$, and $U^{91+}(1s)-U^{92+}$ collisions is investigated. We demonstrated, that the relativistic and nonrelativistic charge-transfer probabilities as functions of the impact parameter have the same oscillatory behavior at low energies, but the relativistic curve shifted to lower energies compared to the nonrelativistic one. In the case of the $U^{91+}(1s)-U^{92+}$ collision the relativistic effect reduces the values of the cross section by about 30%.

In our further investigations we plan to study in more details the effect of diving the $1\sigma_g$ level of the U_2^{183+} quasi-molecule into the negative-energy Dirac spectrum and the influence of this effect on the values of the charge-transfer probability. With this goal, we are going to develop an approach which would allow us to compare the calculated probabilities with and without the diving of the ground state into the negative-energy continuum. We also plan to extend our method to collisions involving many-electron ions and neutral atoms. This will allow us to study the $1s-1s$ charge transfer in low-energy heavy ion-atom collisions. Such experiments, that were successfully performed for low- and middle- Z collisions [99–102], are presently under preparation for high- Z collisions at GSI.

Acknowledgments

We thank V. Shevelko for providing us with his PWB results for the charge-transfer probabilities and for valuable discussions. This work was supported by DFG (Grants No. 436RUS113/950/0-1 and VO 1707/1-1), by GSI, by RFBR (Grants No. 08-02-91967 and 10-02-00450), by the Ministry of Education and Science of Russian Federation (Program for Development of Scientific Potential of High School, Grant No. 2.1.1/1136; Program “Scientific and pedagogical specialists for innovative Russia”, Grant No. P1334), and by the ExtreMe Matter Institute EMMI in the framework of the Helmholtz Alliance HA216/EMMI. Y.S.K. acknowledges financial support by the Dynasty Foundation and DAAD. V.M.S. acknowledges financial support by the Alexander von Humboldt Foundation.

-
- [1] O.B. Firsov, Zh. Eksp. Teor. Fiz. **21**, 1001 (1951).
 - [2] Yu.N. Demkov, Uchen. Zap. Leningr. Univ. **146**, 74 (1952).
 - [3] D.R. Bates, H.S.W. Massey, and A.L. Stewart, Proc. Roy. Soc (London) **A216**, 437 (1953).
 - [4] B.H. Bransden and M.R.C. Mcdowell, *Charge Exchange and the Theory of Ion-Atom Collisions*, (Oxford University Press, NY 1992).
 - [5] W. Fritsch and C.D. Lin, Phys. Rep. **202**, 1 (1991).
 - [6] T.G. Winter, Adv. At. Mol. Opt. Phys. **52**, 391 (2005).
 - [7] D.F. Gallaher, L. Wilets, Phys. Rev. **169**, 139 (1968).
 - [8] R. Shakeshaft, Phys. Rev. A **14**, 1626 (1976).
 - [9] J.F. Reading, A.L. Ford and R.L. Becker, J. Phys. B **14** 1995 (1981).
 - [10] W. Fritsch, C.D. Lin, Phys. Rev. A **27**, 3361 (1983).
 - [11] A.M. Ermolaev, J. Phys. B **23**, L45 (1990).
 - [12] N. Toshima, Phys. Rev. **59**, 1981 (1999).
 - [13] T.G. Winter, Phys. Rev. A **80**, 032701 (2009).
 - [14] N. Grün, A. Mühlhans and W. Scheid, J. Phys. B **15**, 4043 (1982).
 - [15] A. Kolakowska, M.S. Pindzola, F. Robicheaux, D.R. Schultz, C. Wells, Phys. Rev. A **98**, 2872 (1998).
 - [16] A. Kolakowska and M.S. Pindzola, D.R. Schultz, Phys. Rev. A **59**, 3588 (1999).
 - [17] D.R. Schultz, M.R. Strayer and J.C. Wells, Phys. Rev. Lett. **82**, 3976 (1999).
 - [18] X. Tong, D. Kato, T. Watanabe, and S. Ohtani Phys. Rev. A **62**, 052701 (2000).
 - [19] J.S. Briggs, and J.H. Macek, J. Phys. B **6**, 982 (1973); Corrigenda **6**, 2484 (1973).
 - [20] J. Eichler and W.E. Meyerhof, *Relativistic Atomic Collisions*, (Academic, New York, 1995).
 - [21] V.M. Shabaev, Phys. Rep. **356**, 119 (2002).
 - [22] J. Eichler and T. Stöhlker, Phys. Rep. **439**, 1 (2007).
 - [23] Y.B. Zeldovich and V.S. Popov, Usp. Fiz. Nauk **105**, 403 (1971) [Sov. Phys. Usp. **14**, 673 (1972)].
 - [24] J. Rafelski, L.P. Fulcher, and W. Greiner, Phys. Rev. Lett. **27**, 958 (1971).
 - [25] W. Greiner, B. Müller, J. Rafelski, *Quantum Electrodynamics of Strong Fields*, (Springer-Verlag, Berlin, 1985).

- [26] U. Müller-Nehler and G. Soff, Phys. Rep. **246**, 101 (1994).
- [27] J. Rafelski, B. Müller, Phys. Lett. **65B**, 205 (1976).
- [28] J. Eichler, *Lectures on Ion-Atom Collisions: From Nonrelativistic to Relativistic Collisions*, (Elsevier, Amsterdam, 2005).
- [29] U. Becker, N. Grün, W. Scheid, and G. Soff, Phys. Rev. Lett. **56**, 2016 (1986).
- [30] M.R. Strayer, C. Bottcher, V.E. Oberacker, and A.S. Umar, Phys. Rev. A **41**, 1399 (1990).
- [31] J. Thiel, A. Bunker, K. Momberger, N. Grün, and W. Scheid, Phys. Rev. A **46**, 2607, (1992).
- [32] K. Momberger, A. Belkacem, and A.H. Sorensen, Phys. Rev. A **53**, 1605 (1996).
- [33] J.C. Wells, V.E. Oberacker, M.R. Strayer, and A.S. Umar, Phys. Rev. A **53**, 1498 (1996).
- [34] D.C. Ionescu and A. Belkacem, Physica Scripta **T80**, 128 (1999).
- [35] M.S. Pindzola, Phys. Rev. A **62**, 032707 (2000).
- [36] O. Busic, N. Grün, and W. Scheid, Phys. Rev. A **70**, 062707 (2004).
- [37] J. Eichler, Phys. Rep. **193**, 165 (1990).
- [38] K. Rumrich, G. Soff, W. Greiner, Phys. Rev. A **47**, 215 (1993).
- [39] K. Momberger, N. Grün, and W. Scheid, J. Phys. B **26**, 1851 (1993).
- [40] M. Gail, N. Grün and W. Scheid, J. Phys. B **36**, 1397 (2003).
- [41] G. Soff, J. Reinhardt, and W. Betz, Phys. Scr. **17**, 417 (1978).
- [42] T.H.J de Reus, J. Reinhardt, B. Müller, W. Greiner, G. Soff, and U. Müller, J. Phys. B **17**, 615 (1984).
- [43] E. Ackad and M. Horbatsch, Phys. Rev. A **78**, 062711 (2008).
- [44] Th. Stöhlker, D.C. Ionescu, P. Rymuza, F. Bosch, H. Geissel, C. Kozhuharov, T. Ludziejewski, P.H. Mokler, C. Scheidenberger, Z. Stachura, A. Warczak and R. W. Dunford, Phys. Lett. A **238**, 43 (1998).
- [45] Th. Stöhlker, D.C. Ionescu, P. Rymuza, Z. Stachura, A. Warczak, and R. W. Dunford, Phys. Rev. A **57**, 845 (1998).
- [46] D.C. Ionescu and Th. Stöhlker, Phys. Rev. **67**, 022705 (2003).
- [47] M. Rotenberg, Adv. At. and Mol. Phys. **6**, 233 (1970).
- [48] P.F. Gruzdev, G.S. Soloveva, A.I. Sherstyuk, Opt. and Spectrosc, **63**, 1394 (1987),
- [49] N.L. Manakov, L.P. Rapoport and S.A. Zapryagaev, Phys. Lett. A **43**, 139 (1973).
- [50] G.W.F. Drake and S.P. Goldman, Adv. At. Mol. Phys. **25**, 393 (1988).
- [51] J. Avery and F. Antonsen, J. Math. Chem. **24**, 175 (1998).

- [52] I.P. Grant and H.M. Quiney, Phys. Rev. A **62**, 022508 (2000).
- [53] I.I. Tupitsyn, V.M. Shabaev, J.R. Crespo López-Urrutia, I. Draganic, R. Soria Orts, and J. Ulrich, Phys. Rev. A **68**, 022511 (2003).
- [54] I.I. Tupitsyn, A.V. Volotka, D.A. Glazov, V.M. Shabaev, G.Plunien, J.R.Crespo Lopez-Urrutia, A.Lapierre, and J. Ullrich, Phys. Rev. A **72**, 062503 (2005).
- [55] P.O. Löwdin, Adv. in Phys. **5**, 1 (1956).
- [56] S. Kotochigova, I. Tupitsyn, Int. J. Quantum Chem. **29**, 307 (1995).
- [57] I.I. Tupitsyn, D.A. Savin, and V.G. Kuznetsov, Opt. and Spectrosc. **84**, 344 (1998).
- [58] L. Yang, D. Heinemann, D. Kolb, Chem. Phys. Lett. **178**, 213 (1991).
- [59] O. Kullie, D. Kolb, Eur. Phys. J. D **17**, 167 (2001).
- [60] V.I. Lisin, M.S. Marinov, V.S. Popov, Phys. Lett. **69B**, 2 (1977).
- [61] V.I. Matveev, D.U. Matrasulov, and H.Yu. Rakhimov, Phys. At. Nucl. **63**, 318. (2000).
- [62] B. Müller, and W. Greiner, Z. Naturforsch. **31a**, 1 (1976).
- [63] V.I. Lisin, M.S. Marinov, V.S. Popov, Phys.Lett. **91B**, 20 (1980).
- [64] V.S. Popov, Phys. At. Nucl. **64**, 367, (2001).
- [65] J. Crank, P. Nicholson, Proc. Cambridge Philos. Soc. **43**, 50 (1947).
- [66] M.D. Feit, J.A. Fleck, Jr., and A. Steiger, J. Comput. Phys. **47**, 412 (1982).
- [67] J. Wilkinson, C. Reinsch, *Handbook for Automatic Computation*, (Springer-Verlag, Berlin, 1971),
- [68] I.P. Grant, B.L. Gyorffy, *The Effects of Relativity in Atoms, Molecules, and the Solid State*, (ed. S Wilson, New York: Plenum, 1991).
- [69] R. Szmytkowski, J. Phys. B **30**, 825 (1997).
- [70] I.P. Grant, Adv. Phys. **19**, 747 (1970).
- [71] V.F. Bratsev, G.B. Deyneka, and I.I. Tupitsyn, Bull.Acad.Sci. USSR, Phys. Ser. **41**, 173 (1977).
- [72] R.R. Sharma, Phys. Rev. A **13**, 517 (1977).
- [73] M.E. Rose, *Relativistic Electron Theory*, (John-Wiley & Sons, NY-London, 1961)
- [74] D.A. Varshalovich, A.N. Moskalev, V.K. Khersonskii, *Quantum Theory of Angular Momentum*, (World Scientific, Singapore, 1988).
- [75] J.E. Marsden, A.J. Tromba, *Vector Calculus*, (5th edition, W.H. Freeman & Company, New-York, 2003).
- [76] E.U. Condon, G.H. Shortley, *Theory of Atomic Spectra*, (Cambridge University Press, London, 1935).

- [77] V.M. Shabaev, I.I. Tupitsyn, V.A. Yerokhin, G. Plunien, and G. Soff, Phys. Rev. Lett. **93**, 130405 (2004).
- [78] I.I. Tupitsyn, V.M. Shabaev, Opt. and Spectrosc. **105**, 183 (2004).
- [79] F.A. Parpia, A.K. Mohanty, Chem. Phys. Lett. **238**, 209 (1995).
- [80] L. LaJohn, J.D. Talman, Theor. Chim. Acta. **99**, 351 (1998).
- [81] A. Rutkowski, Chem. Phys. Lett. **307**, 259 (1999).
- [82] B. Müller, J. Rafelski, and W. Greiner, Z. Physik **257**, 183 (1972).
- [83] M.S. Marinov, V.S. Popov, and V.L. Stolin, J. Comp. Phys. **19**, 241 (1975).
- [84] K-H Wietschorke, B. Muller, W. Greiner and G. Soff, J. Phys. B **12**, L31 (1979).
- [85] F.A. Parpia, A.K. Mohanty, Phys. Rev. A **46**, 3735 (1992).
- [86] I. Angeli, At. Data Nucl. Data Tables **87**, 185 (2004).
- [87] Y.S. Kozhedub, V.M. Shabaev, unpublished.
- [88] Y.S. Kozhedub, O.V. Andreev, V.M. Shabaev, I.I. Tupitsyn, C. Brandau, C. Kozhuharov, G. Plunien, and T. Stöhlker, Phys. Rev. A **77**, 032501 (2008).
- [89] W.R. Johnson, G. Soff, At. Data Nucl. Data Tables **33**, 405 (1985).
- [90] W. Fritsch and C.D. Lin, Phys. Rev. A **26**, 762 (1982).
- [91] H.J. Lüdde and R.M. Dreizler, J. Phys. B **14**, 2191 (1981).
- [92] H.J. Lüdde and R.M. Dreizler, J. Phys. B **15**, 2703 (1982).
- [93] R. Shakeshaft, Phys. Rev. A **18**, 1930 (1978).
- [94] R.K. Janev, J.J. Smith, Atomic and Plasma Material Interaction Data for Fusion, Nucl Fusion Suppl. Special Issue, **4** (1993).
- [95] M.B. Shah J. Phys. B **20**, 2481 (1987).
- [96] M.B. Shah J. Phys. B **31**, L757 (1998).
- [97] V.P. Shevelko, private communication.
- [98] V.P. Shevelko, I.Yu. Tolstikhina, Th. Stöhlker, Nucl. Instrum. Methods B **184**, 295 (2001).
- [99] S. Hagmann, C. L. Cocke, J. R. Macdonald, P. Richard, H. Schmidt-Böcking, and R. Schuch, Phys. Rev. A **25**, 1918 (1982).
- [100] S. Hagmann, S. Kelbch, H. Schmidt-Böcking, C. L. Cocke, P. Richard, R. Schuch, A. Skutlartz, J. Ullrich, B. Johnson, M. Meron, K. Jones, D. Trautmann and F. Rösel, Phys. Rev. A **36**, 2603 (1987).
- [101] R. Schuch, H. Ingwersen, E. Justiniano, H. SchmidtBocking, M. Schulz, and F. Ziegler, J. Phys. B **17**,

2319 (1984).

- [102] R. Schuch, M. Meron, B. M. Johnson, K. W. Jones, R. Hoffmann, H. Schmidt-Böcking, I. Tserruya, Phys. Rev. A **37**, 3313 (1988).